

# Bacterio- and Isobacteriodilactones by Stepwise or Direct Oxidations of *meso*-Tetrakis(pentafluorophenyl)porphyrin

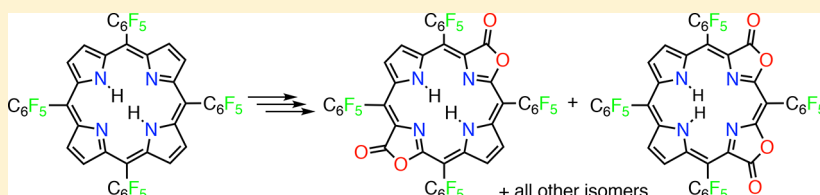
Nisansala Hewage,<sup>†,||</sup> Pedro Daddario,<sup>†,||</sup> Kimberly S. F. Lau,<sup>†,‡,||</sup> Matthew J. Guberman-Pfeffer,<sup>†</sup> José A. Gascón,<sup>†,ID</sup> Matthias Zeller,<sup>§,ID</sup> Christal O. Lee,<sup>‡</sup> Gamal E. Khalil,<sup>‡</sup> Martin Gouterman,<sup>‡</sup> and Christian Brückner<sup>\*,†,ID</sup>

<sup>†</sup>Department of Chemistry, University of Connecticut, Unit 3060, Storrs, Connecticut 06269-3060, United States

<sup>‡</sup>Department of Chemistry, University of Washington, Box 351700, Seattle, Washington 98195, United States

<sup>§</sup>Department of Chemistry, Purdue University, 101 Wetherill Hall, 560 Oval Drive, West Lafayette, Indiana 47907-2084, United States

## Supporting Information



**ABSTRACT:** Porpholactones are porphyrinoids in which one or more  $\beta,\beta'$ -bonds of the parent chromophore were replaced by lactone moieties. Accessible to varying degrees by direct and nonselective oxidations of porphyrins, the rational syntheses of all five dilactone isomers along stepwise, controlled, and high-yielding routes via porphyrin  $\rightarrow$  tetrahydroxyisobacteriochlorin metal complexes  $\rightarrow$  isobacteriochlorindilactone metal complexes or porphyrin  $\rightarrow$  tetrahydroxybacteriochlorin  $\rightarrow$  bacteriochlorindilactone (and related) pathways, respectively, are described. A major benefit of these complementary routes over established methods is the simplicity of the isolation of the dilactones because of the reduced number of side products formed. In an alternative approach we report the direct and selective conversion of free base *meso*-tetrakis(pentafluorophenyl)porphyrin to all isomers of free base isobacteriodilactones using the oxidant cetyltrimethylN<sup>+</sup>MnO<sub>4</sub><sup>-</sup>. The solid-state structures of some of the isomers and their precursors are reported, providing data on the conformational modulation induced by the derivatizations. We also rationalize computationally their differing thermodynamic stability and electronic properties. In making new efficient routes toward these dilactone isomers available, we enable the further study of this diverse class of porphyrinoids.

## INTRODUCTION

Porphyrin-like molecules containing nonpyrrolic building blocks, the so-called pyrrole-modified porphyrins (PMPs),<sup>1</sup> possess altered optical (electronic) and chemical properties compared to regular porphyrins and hydroporphyrins.<sup>2</sup> A wide structural variety of PMPs is available.<sup>1,2</sup>

Porpholactones, such as the *meso*-tetrakis(pentafluorophenyl) derivative **2**, are derived from porphyrin **1** by replacement of a pyrrolic  $\beta,\beta'$ -bond by a lactone moiety and are, for their particular versatility, one of the more widely studied classes of PMPs.<sup>2c</sup> Their free bases and metal complexes have found uses as model compounds for naturally occurring prosthetic groups,<sup>3</sup> as chlorophyll models,<sup>4</sup> for nitrogen transfer,<sup>5</sup> sulfoxidation,<sup>6</sup> and olefin epoxidation catalysts,<sup>7</sup> as photocatalysts for oxidative C–H functionalization,<sup>8</sup> as a component in pressure-sensitive paints,<sup>9</sup> as bioimaging agents,<sup>10</sup> as optical cyanide sensors,<sup>11</sup> as catalysts for the electrochemical hydrogen evolution reaction,<sup>12</sup> and as optical ratiometric high-pH sensors.<sup>13</sup> The lanthanide sensitization efficiency of porpholactones exceeds those of the corresponding porphyrins.<sup>10</sup> The lactone moiety of a

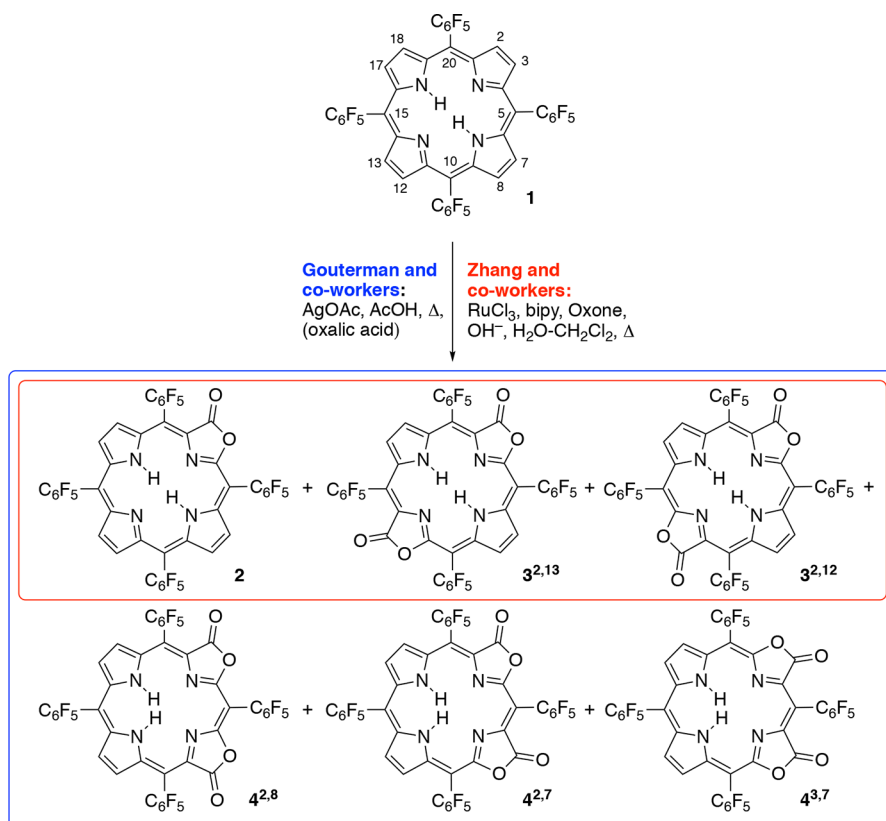
porpholactone-based photosensitizer also enhances the lipoprotein binding affinity, cellular uptake, and intracellular localization selectivity when compared to the parent porphyrin.<sup>14</sup> Related porpholactone derivatives such as porpholactams and derivatives based on octaalkylporphyrins, carbaporphyrins, or subporphyrins<sup>15</sup> are known.<sup>2c</sup>

Since their discovery in 1984 by adventitious oxidation of *meso*-tetraphenylporphyrin,<sup>18</sup> a number of oxidative pathways have been described that generate porpholactones from nonderivatized *meso*-arylporphyrins as well as  $\beta$ -derivatized porphyrins or chlorins.<sup>2c,19</sup> In fact, porpholactones appear to be fairly common *meso*-arylporphyrin oxidation products. This is remarkable since no porpholactone-like compounds were observed to form during the regular oxidative degradation pathways of the naturally occurring  $\beta$ -alkylated porphyrins and chlorins.<sup>20</sup> No total syntheses of porpholactones have become known.

Received: October 11, 2018

Published: November 28, 2018

**Scheme 1. Direct Conversion of *meso*-Tetrakis(pentafluorophenyl)porphyrin to Porpholactone and Porphodilactones According to Gouterman and Co-workers<sup>16</sup> and Zhang and Co-workers<sup>17</sup>**



*meso*-(C<sub>6</sub>F<sub>5</sub>)-porphyrin **1** was the first  $\beta$ -unsubstituted porphyrin that allowed its direct oxidation to monoderivatized porpholactone **2**.<sup>16</sup> However, the oxidation was not selective and did not stop after the oxidation of one  $\beta\beta'$ -bond; consequently, all of the five possible regiosomeric dilactones were formed (Scheme 1).<sup>16</sup> Using alternative oxidants, primarily monolactone **2** and dilactones **3<sup>2,13</sup>** and **3<sup>2,12</sup>** were observed.<sup>17,21</sup>

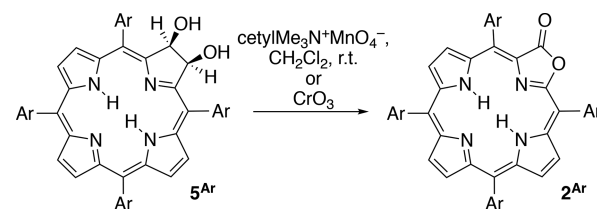
The regiosomeric dilactones fall into two classes: The compounds **3<sup>2,13</sup>** and **3<sup>2,12</sup>** possess bacteriochlorin-type substitution patterns ( $\beta$ -positions of opposite pyrrolic moieties were modified); we will refer to them as bacteriodilactones.<sup>22</sup> The three regiosomers **4<sup>2,8</sup>**, **4<sup>2,7</sup>**, and **4<sup>3,7</sup>** possess isobacteriochlorin-like substitution patterns ( $\beta$ -positions of adjacent pyrrolic moieties were modified); we thus will refer to them as isobacteriodilactones. The naming is purely based on structure and does not imply that these chromophores necessarily possess bacteriochlorin- or isobacteriochlorin-like optical spectra/electronic properties. The strong electronic influence of the lactone moieties on the electronic structure of the chromophore was the subject of earlier studies.<sup>16,23</sup>

All dilactones lay virtually dormant for 25 years. Zhang and co-workers can be credited for having rediscovered the intriguing bacteriodilactones.<sup>4</sup> They developed an efficient one-step synthesis (Scheme 1). Crucially, they achieved the separation of the two bacteriochlorin-type isomers **3<sup>2,13</sup>** and **3<sup>2,12</sup>** as their zinc(II) complexes and studied the photophysical differences of the two isomers.<sup>4</sup> Compared to the NIR-absorbing bacteriochlorins, the more hypsochromically absorbing isobacteriochlorins have generally been much less studied.<sup>25</sup> This is also the case for the isobacteriodilactone

isomers **4**; we are not aware of their detailed study beyond their initial discovery and cursory description.<sup>16</sup>

Based on our stepwise, controlled, and high-yielding preparation of porpholactones via a porphyrin  $\rightarrow$  dihydroxychlorin **5<sup>Ar</sup>**  $\rightarrow$  porpholactone **2<sup>Ar</sup>** two-step oxidation pathway (Scheme 2),<sup>23,26</sup> we report here the rational and stepwise

**Scheme 2. Literature-Known Syntheses of Porpholactones by Oxidation of Dihydroxychlorins **5<sup>Ar</sup>**<sup>23,26</sup>**



synthesis of the bacteriodilactone isomers along porphyrin  $\rightarrow$  tetrahydroxybacteriochlorin  $\rightarrow$  bacteriodilactones (and related) routes. Compared to the established methods, one major benefit of this complementary route is the simplicity of the isolation of the bacteriodilactones because of the much reduced number of (side)products formed.

We also report details on the synthesis of tetrahydroxyisobacteriochlorin metal complexes (M = Zn<sup>2+</sup>, Pt<sup>2+</sup>) and their conversion to metalloisobacteriodilactones **4** along the route [dihydroxychlorin]M **5M**  $\rightarrow$  [tetrahydroxyisobacteriochlorin]M **13M**  $\rightarrow$  [isobacteriodilactones]M **4M** (and related) routes. We were able to separate and characterize all regiosomeric metalloisobacteriodilactones and computationally describe their varying electronic structures. Lastly, we

**Scheme 3. OsO<sub>4</sub>-Mediated Dihydroxylation of Free Base *meso*-(C<sub>6</sub>F<sub>5</sub>)-Porphyin 1 to the Corresponding Dihydroxychlorins 6/5 and Tetrahydroxybacteriochlorins 7/8<sup>27b,c</sup>**

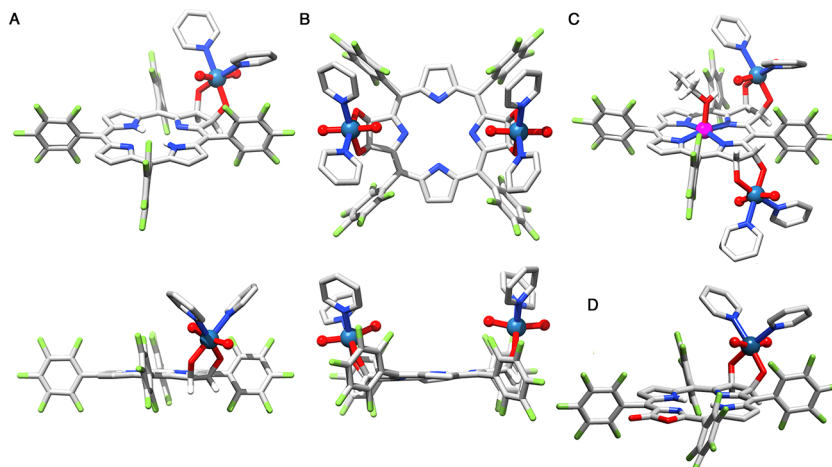
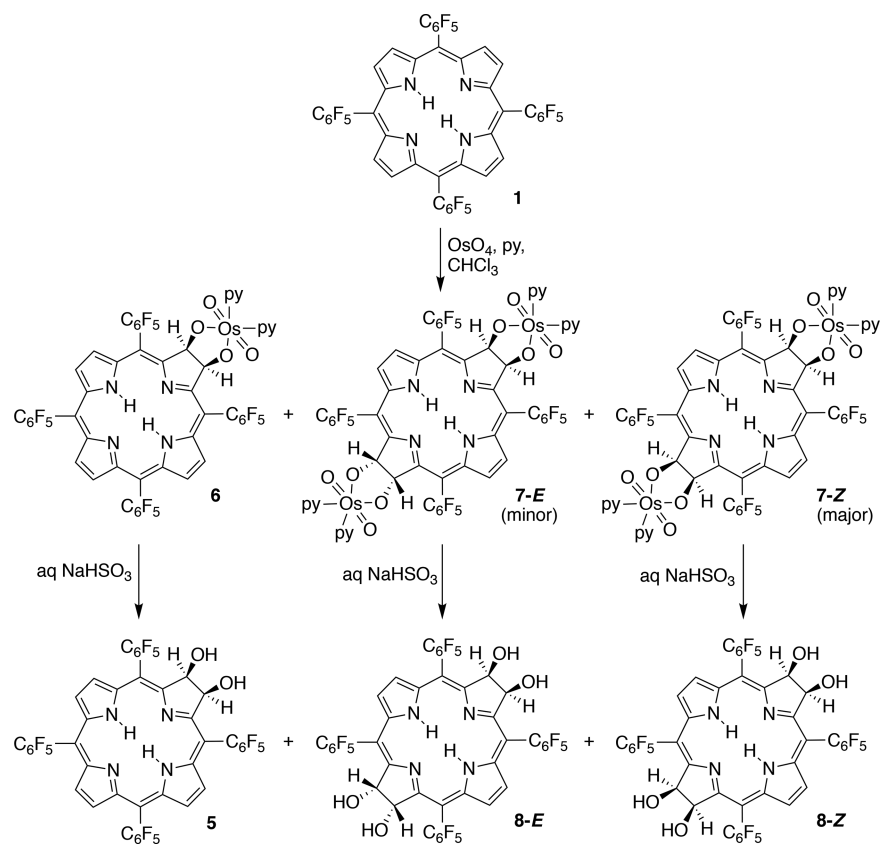


**Figure 1.** Stick representation of the X-ray single-crystal structures of (A) dihydroxychlorin osmate ester 6 (oblique and side views), (B) tetrahydroxybacteriochlorin bisosmate ester 7-*Z* (top and side views), (C) [tetrahydroxyisobacteriochlorinato]Zn-EtOH bisosmate ester 12Zn-*E* (oblique view), and (D) dihydroxybacteriolactone osmate ester 9 (oblique view). All disorder, all hydrogen atoms bonded to sp<sup>2</sup>-carbons, and solvents (if present) are removed for clarity; only one of two independent molecules in the crystal is shown, if present.

discovered that the direct and selective conversion of free base porphyrin 1 to all isomers of free base isobacteriolactones 4 using MnO<sub>4</sub><sup>-</sup> as an oxidant is also possible. Some of the products or intermediates were structurally characterized, providing certainty of the structural assignments of the isomers and providing information on the conformation of these pyrrole-modified porphyrins. In presenting these complementary routes toward the dilactones, we contribute to the understanding of the regiochemistry of multiple pyrrole

modifications and make the dilactones more readily available for further study.

## RESULTS AND DISCUSSION

### Dihydroxylation of Free-Base *meso*-(C<sub>6</sub>F<sub>5</sub>)-Porphyrin

1. The OsO<sub>4</sub>-mediated dihydroxylation of free base *meso*-(C<sub>6</sub>F<sub>5</sub>)-porphyrin 1 to the corresponding dihydroxychlorin 5 and tetrahydroxybacteriochlorin isomers 8-*E* (both diol pairs pointing to the same hemisphere defined by the mean plane of

the macrocycle) and **8-Z** (both diol pairs pointing to opposite sides) was described previously (**Scheme 3**).<sup>27</sup> The reaction deserves mention here only for our finding that the intermediate osmate esters **7**, previously not isolated but directly reduced to the corresponding diols, are chemically stable, readily chromatographed, and purified. In fact, osmate esters **7** are more robust than the sensitive and hard to purify bacteriochlorin tetraols **8**. They could be spectroscopically and structurally characterized (**Figure 1**). The ability to reduce the osmate esters to the corresponding diols, including for *meso*-C<sub>6</sub>F<sub>5</sub>-substituted hydroporphyrinoids (e.g., reduction of **7** to **8**), was shown previously.<sup>27</sup> A general disadvantage of the osmate esters is, however, that the molecular ions proved in our hands to be intractable toward mass spectrometric analysis (using ESI+ and ESI+, FAB, DART, EI, and MALDI ionization techniques), nor could we derive consistent fragmentation patterns.

The crystal structure of the chlorin diol osmate ester shows the configuration of the osmate ester with an octahedrally coordinated osmium(IV) atom bearing two *trans*-oxo groups; the configuration was also derived from the 2-fold symmetry of the molecules as seen by NMR spectroscopy and observed in other osmate esters.<sup>28</sup> The osmate ester metallacycle(s) in **6** and **7-Z** enforce a near-perfectly eclipsed configuration of the two C<sub>pyrroline</sub>—O<sub>osmate</sub> bonds (dihedral angles of 5–7°). Notable is the extent to which this affects the conformation of the hydroporphyrin macrocycles when compared to the corresponding diols/tetraols or their methyl ethers: The osmate esters are significantly more planar than the corresponding diol or tetraols that exhibit dihedral angles of 17° (between neighboring C<sub>pyrroline</sub>—OH(Me) bonds) in a structurally characterized chlorin and between 28 and 30° in bacteriochlorins (**Figure 2**).<sup>27a</sup> This provides proof for the hypothesis

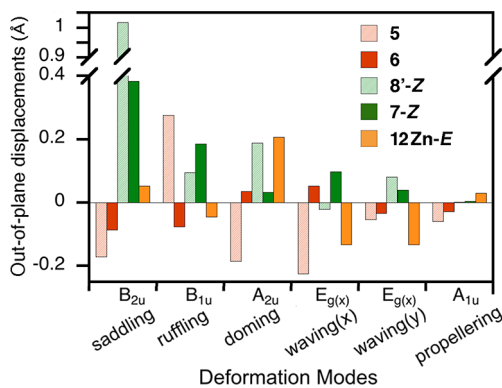


**Figure 2.** NSD analysis of the macrocycle conformation of chlorin diol **5**<sup>27a</sup> and its corresponding chlorin osmate ester **6**, bacteriochlorin tetraol **8'-Z** (Ar = 3,4,5-trimethoxyphenyl),<sup>27a</sup> bacteriochlorin bisosmate ester **7-Z**, and isobacteriochlorin bisosmate ester **12Zn-E**.

advanced previously<sup>27a</sup> that the hydroporphyrin macrocycle conformations are driven by the avoidance of the eclipsed configuration of the pyrroline diol functionalities. Compared to the conformation of their nonosmylated counterparts chlorin **5** and bacteriochlorin **8'-Z**,<sup>27a</sup> the conformations of the chlorin osmate ester **6** and the bacteriochlorin bisosmate ester **7-Z** are, quantitatively, much less distorted from planarity. Qualitatively, the relative weighting of the deformation modes also changes (**Figure 2**).<sup>29</sup>

The minor conformational changes of the chromophores upon introduction of the osmate esters are also noticeable in the slightly shifted optical spectra of the osmate esters compared to the spectra of the corresponding alcohols, whereby the shifts for the conformationally slightly more flexible bacteriochlorins are larger (shift of  $\lambda_{\text{max}}$  of 5 nm) than those for the chlorins (shift of  $\lambda_{\text{max}}$  of 2 nm) (**Figure 3**).

**Conversion of Chlorin Osmate Ester **6** to Porpholactone **2**.** Similarly to the well-known conversion of dihydroxychlorin **5** to porpholactone **2**,<sup>23</sup> chlorin osmate ester **6** is a suitable substrate for this oxidation, with no need for an adjustment of the reaction conditions (**Scheme 4**). Since both the diols and the corresponding esters are equally suited for their conversions to lactone moieties, we will discuss in the remainder of this report their oxidation interchangeably, but with a focus on using the more robust osmate esters. *meso*-Phenyl-substituted porphyrins also undergo the step-by-step modifications described here,<sup>30</sup> but the much greater solubility of the *meso*-(C<sub>6</sub>F<sub>5</sub>)-substituted derivatives facilitates their handling. We will detail here exclusively the chemistry of the C<sub>6</sub>F<sub>5</sub> derivatives.

**Dihydroxylation of *meso*-Tetrakis(pentafluorophenyl)porpholactone **2**.** Reaction of porpholactone **2** under standard porphyrin osmylation conditions (1.1 equiv of OsO<sub>4</sub> in CHCl<sub>3</sub> at ambient conditions in the presence of pyridine)<sup>27</sup> converted it nearly quantitatively into a single, new, more polar product as smoothly and as swiftly (24 h) as porphyrin **1**.

The UV-vis spectrum of the product **9** is chlorin-like but significantly red-shifted compared to chlorin diol **5** or its osmate ester **6** (**Figure 4**) and similar to that of known dihydroporpholactone (chlorolactones) **10**<sup>31</sup> but notably dissimilar to the spectra of hydroporpholactone **11**<sup>32</sup> reduced at a pyrrole adjacent to the pyrrolinone (see also below). This suggests that  $\beta,\beta'$ -dihydroxylation of **2** had taken place at the pyrrole opposite the pyrrolinone moiety, characterizing free base porpholactone with respect to the dihydroxylation regioselectivity as a typical free base chlorin;<sup>33</sup> alas, not all chlorins show this regiochemistry in, for example, cycloadditions to the  $\beta,\beta'$ -bond.<sup>33b</sup> A crystal structure analysis of osmate ester **9** also supports this structural assignment (**Figure 1**).

**Oxidations of Tetrahydroxybacteriochlorin **8**, Its Osmate Ester **7**, and Dihydroxybacteriolactone Osmate Ester **9**.** The two different oxidants (cetylMe<sub>3</sub>N<sup>+</sup>MnO<sub>4</sub><sup>-</sup> or CrO<sub>3</sub>)<sup>23,26</sup> suitable for the conversion of dihydroxychlorin **5** to porpholactones **2** are also suited for the oxidation of tetrahydroxybacteriochlorins **8**, osmate ester **7-E** (or a mixture of **7-E** and **7-Z**), or dihydroxychlorolactone osmate ester **9**, generating in all cases a mixture of the two known<sup>4,16</sup> bacteriolactones **3**<sup>2,13</sup> and **3**<sup>2,12</sup> in about a 1:0.7 ratio (and, depending on the substrate and oxidant, between 40 and 60% yield). Notably, this ratio is different than the 0.4:1 (**3**<sup>2,13</sup>:**3**<sup>2,12</sup>) ratio of the products reported by Zhang and co-workers.<sup>4</sup> The separation of the mixture of the nonpolar bacteriolactones from the polar side products, excess oxidant, and the oxidant-related products is facile. Careful reaction control is recommended, however; excessive reaction times or a large stoichiometric excess of the oxidant leads rapidly to a degradation of the yield. The straightforward NMR-spectroscopic analysis of the products is based on the differing symmetry of the products (**3**<sup>2,13</sup> possesses idealized C<sub>2v</sub> and **3**<sup>2,12</sup> C<sub>2h</sub> point group symmetry) (see the SI).<sup>4</sup> The Zhang

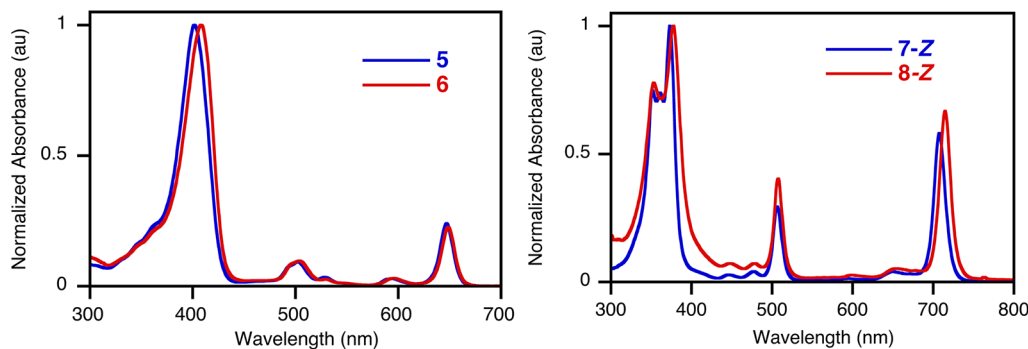


**Figure 3.** UV-vis absorption (solid line)  $\text{CH}_2\text{Cl}_2$  of dihydroxychlorin **5**, its corresponding osmate ester **6**, tetrahydroxybacteriochlorin **8-Z** and its corresponding osmate ester **7-Z**.

**Scheme 4. Synthetic Pathways toward Regioisomeric Mixtures of Bacteriodilactones **3****

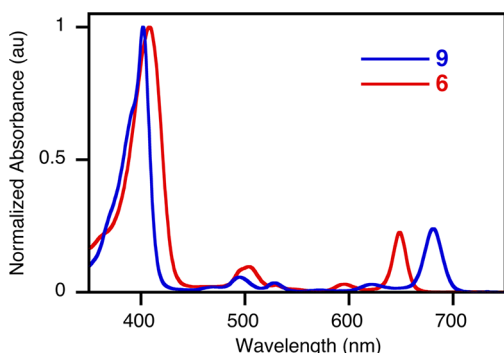
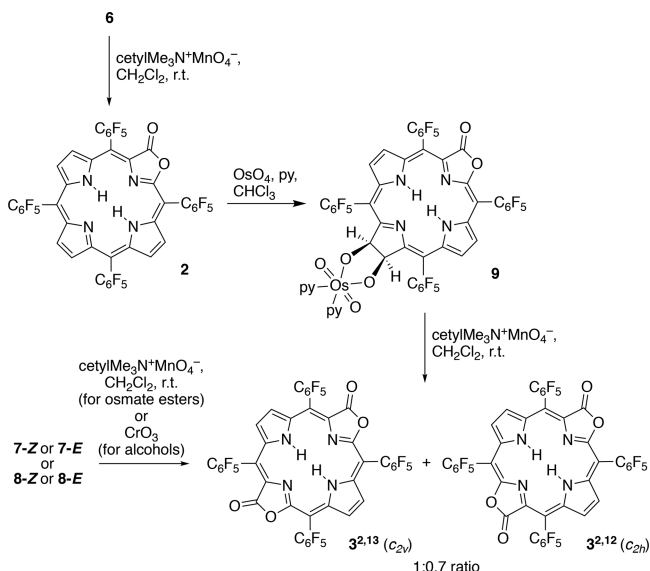
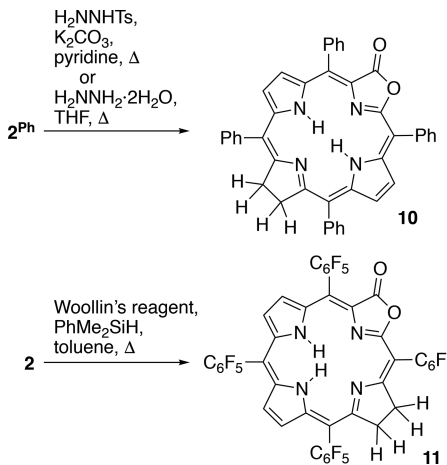


**Figure 4.** UV-vis absorption of dihydroxybacteriolactone osmate ester **9** in comparison to that of the parent dihydroxychlorin osmate ester **6**.

group has shown the separation of the two regioisomers as their zinc complexes.<sup>4</sup>

**Dihydroxylation of [meso-( $\text{C}_6\text{F}_5$ )-porphyrinato]M **1M**.** The standard  $\text{OsO}_4$ -mediated hydroxylation of the zinc(II) or platinum(II) complexes of porphyrin **1**, complexes **1Zn** or **1Pt**, using 1.1 equiv of  $\text{OsO}_4$  forms the corresponding metal complexes of the stable diol chlorin osmate esters **6M** in yields of around 60% (Scheme 6). Except for the isolation and

**Scheme 5. Literature-Known Conversions of Porpholactones **2**/**2<sup>Ph</sup>** to the Corresponding Hydroporpholactones<sup>31,32</sup>**



characterization of the intermediate osmate esters, the dihydroxylation of the Zn(II), Ni(II), Pd(II), and Pt(II) complexes of **2** was reported previously.<sup>27b</sup>

When 2.2 equiv of  $\text{OsO}_4$  are used, only one major blue bisosmate ester product (60% isolated yield at a 1.0 mmol scale) is formed, identified as the isobacteriochlorin-type bisosmate ester **12M-E** by virtue of its metalloisobacteriochlorin-like UV-vis absorption spectra that are hypsochromically shifted compared to those of the corresponding chlorins (Figure 5).<sup>25</sup> Further support for this can be derived from their NMR spectra (Figure 6 and SI). For instance, the  $^{19}\text{F}$  NMR spectrum of the major product identifies four nonequivalent *o*-F, four *m*-F, and three *p*-F atom signal sets, suggesting the *E*-configuration of the two osmate esters (idealized  $C_2$  point group symmetry); the *Z*-configuration (idealized  $C_s$  symmetry) would have generated six *o*-F, six *m*-F, and three *p*-F atom signal sets.  $^1\text{H}$ ,  $^{19}\text{F}$  and  $^{19}\text{F}$ ,  $^{19}\text{F}$  correlation NMR spectra allow the unequivocal assignment of the  $^1\text{H}$  and  $^{19}\text{F}$  NMR signals in the molecules. The selective formation for the metalloisobacteriochlorin upon reduction of a metallochlorin was observed also for the *meso*-tetraphenyl series<sup>34</sup> and was computationally rationalized by a combination of electronic and steric effects.<sup>33</sup> We did not find any indication that the corresponding tetraol *Z*-isomer of **12M** formed to any appreciable extent, likely because of steric effects favoring the *E*-isomer.

**Scheme 6. OsO<sub>4</sub>-Mediated Dihydroxylation of [meso-(C<sub>6</sub>F<sub>5</sub>)-Porphyrinato]M Metal Complexes to the Corresponding Dihydroxymetalloclochlorin 6M and Tetrahydroxymetallocloisobacteriochlorin Osmate Esters 12M-E and Their Reduction to the Corresponding Tetraols 13M-E**

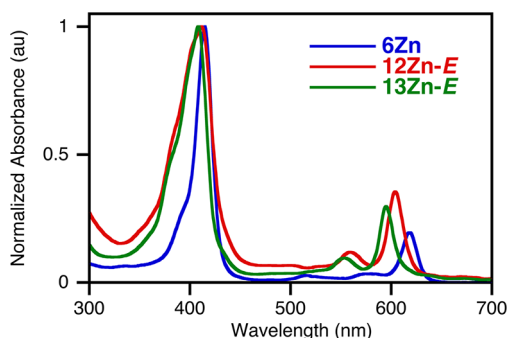
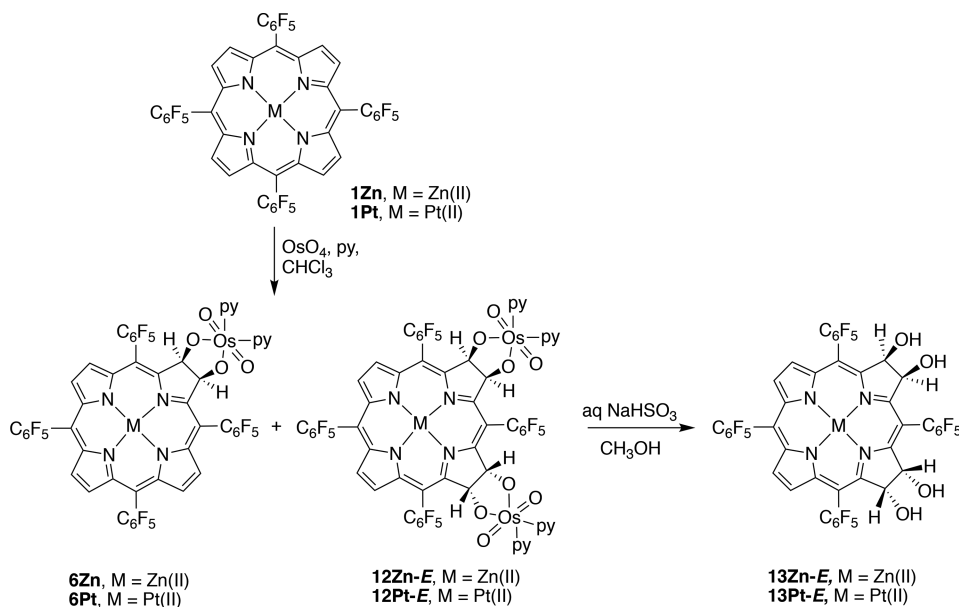


**Figure 5.** UV-vis absorption spectra ( $\text{CH}_2\text{Cl}_2$ ) of the compounds indicated.

The ultimate proof of the connectivity and *E*-stereochemistry of isobacteriochlorin **12Zn-E** was provided by single-crystal X-ray crystallography as its EtOH adduct (Figure 1). The chiral molecule crystallizes as a racemic mixture in the nonchiral space symmetry group  $P\bar{1}$  (for further details, see the SI). The chromophore is only very little distorted from planarity, exhibiting minor doming ( $A_{2u}$ ) and waving ( $E_{g(x)}$  and  $E_{g(y)}$ ) deformation modes of approximately equal magnitude (Figure 2).<sup>29</sup> This is the first X-ray structural characterization of any tetrahydroxysobacteriochlorin derivative, reported first more than 20 years ago.<sup>34</sup>

The reduction of the bisosmate esters **12M-E** to the corresponding tetraols **13M-E** can be accomplished using standard reduction methods.<sup>27b</sup> In the chlorin and bacteriochlorin osmate esters and free alcohol pairs **6/5** and **7/8**, respectively, the osmate esters show slightly blue-shifted optical spectra compared to their free alcohols (Figure 3), but in the isobacteriochlorin, the osmate esters **12M-E** are slightly red-shifted compared to their alcohols **12M-E** (Figure 5), presumably also because of altered conformations.

**Conversion of Metallochlorin Osmate Esters **6M** to Metalloporpholactones **2M**.** Metallochlorin osmate esters **6Zn** and **6Pt** are also competent replacements for their

corresponding alcohols under standard conditions,<sup>23</sup> forming the known metalloporpholactones **2M**<sup>35</sup> in excellent yields (Scheme 7).

**Osmylation of [meso-(C<sub>6</sub>F<sub>5</sub>)-porpholactonato]M(II) **2M**.** Reaction of the metalloporpholactones **2M** with stoichiometric amounts of OsO<sub>4</sub> each form a major product **14M** in good yield (75% isolated yield at a 0.1 mmol scale) (Scheme 7). The UV-vis spectra of the products are metallochlorin-like, similar to that of the corresponding diol chlorin **6M** and ~20 nm red-shifted compared to the spectrum of the corresponding metalloporpholactone **2M** (Figure 7).<sup>25,36</sup>

The <sup>1</sup>H and <sup>19</sup>F NMR spectra of **14M** each suggest the presence of ~1:2 isomeric mixtures of two compounds, assigned to the products resulting from the two possibilities for a derivatization of porpholactones at a pyrrole moiety adjacent to the oxazolone moiety: either the pyrrole facing the oxo-oxygen or the pyrrole on the side of the oxa-oxygen is modified. We could not separate these isomers **14M** or assign with certainty which signal set in the mixture belonged to which isomer.

The isobacteriochlorin-type modification pattern in **14M** resulting from the derivatization of metalloporpholactones **2M**<sup>33</sup> fits the reactivity expectation for regular metallochlorins.<sup>33</sup> Surprisingly, free base isobacterioporpholactone **11**<sup>32</sup> was prepared by Woollin's reagent/silane reduction of free base porpholactone **2**, respectively (see Scheme 5). Moreover, the latter reaction formed regioselectively the compound in which only the pyrroles facing the lactone oxa-groups were derivatized.<sup>32</sup> We conclude therefore that the steric and/or electronic factors controlling the osmylation reaction of porpholactones **2/2M** are principally different from those controlling its reduction.

**Oxidation of Tetrahydroxymetallocloisobacteriochlorin Bisosmate Esters **12M-E**, Dihydroxymetallocloisobacteriolactone Osmate Esters **14M**, or Tetrahydroxymetallocloisobacteriochlorins **13M-E**.** The CTAP-mediated oxidation of either the metalloisobacteriochlorin bisosmate

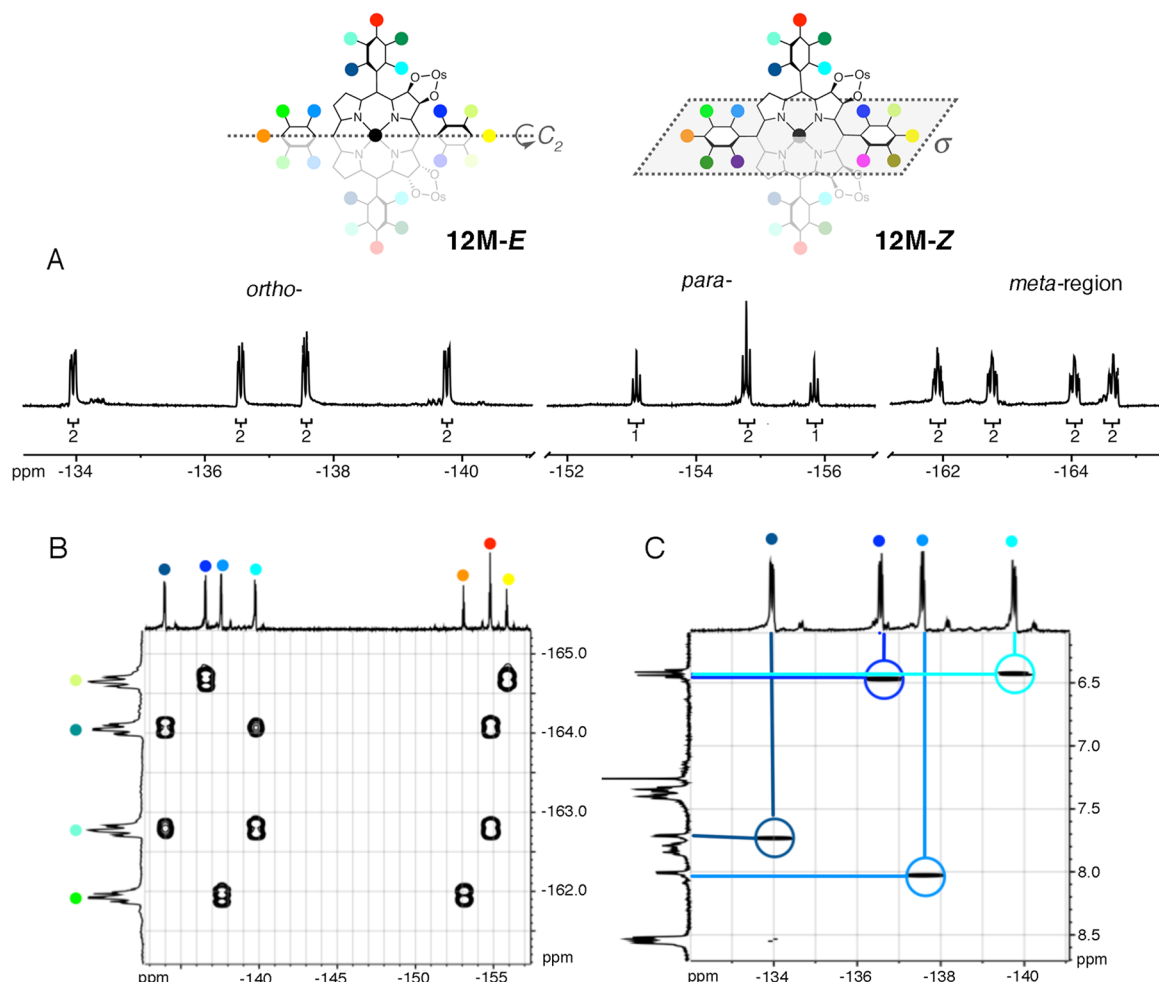


**Figure 6.** (A)  $^{19}\text{F}$  NMR spectrum (376 MHz,  $\text{CDCl}_3$ , 25 °C), (B)  $^{19}\text{F}$ – $^{19}\text{F}$  COSY spectrum (376 MHz,  $\text{CDCl}_3$ , 25 °C), and (C)  $^1\text{H}$ – $^{19}\text{F}$  COSY spectrum (400/376 MHz,  $\text{CDCl}_3$ , 25 °C) of [tetrahydroxyisobacteriochlorinato]platinum(II) bisosmate ester **12Pt-E**, together with drawings of the **12M-E/Z** isomers highlighting their crucial symmetry elements and signal assignments.

ester **12M-E**, its free alcohols **13M-E**, or the metalloisobacteriolactone osmate ester **14M** generated similar fractions of nonpolar and hard-to-separate compounds of identical composition ( $\text{C}_{42}\text{H}_{44}\text{N}_4\text{O}_4\text{M}$ , M = Zn or Pt, as per ESI+ HRMS), corresponding to the expected metalloisobacteriolactones **4M** (Scheme 7). The UV–vis spectra of the mixture of the isomers (Figure 8) are metallochlorin-like and much blue-shifted compared to the spectra of the parent tetrol osmate esters **12Pt** (~50 nm for  $\lambda_{\text{max}}$ ) and **12Zn** (~25 nm for  $\lambda_{\text{max}}$ ), respectively.

As per  $^1\text{H}$ ,  $^{19}\text{F}$ , and  $^{13}\text{C}$  NMR ( $\text{CDCl}_3$ ) analysis, only two of the three possible isobacteriolactone isomers are present in the dilactone fraction obtained from CTAP oxidation, but in unequal amounts: One  $C_{2v}$ -symmetric compound (two d in the pyrrole- $\beta$ -region and a single carbonyl carbon signal), assigned to be isomer  $4^{2,8}\text{M}$ , constituted about 2/3 of the fraction. A  $C_s$ -symmetric compound (three  $\beta$  signals in a 1:2:1 ratio in its  $^1\text{H}$  NMR spectrum), assigned to be  $4^{2,7}\text{M}$ , made up about 1/3 of the fraction, while the second possible  $C_{2v}$ -symmetric isomer,  $4^{3,7}$ , was not observed under these oxidation conditions. The two isomeric products could be separated from each other by preparative TLC (see the SI). For further details on the basis of the assignments of the isomers, see below. The zinc complex **4Zn** could also be demetalated by treatment with acid to

generate the mixture of isomers of free base isobacteriolactone **4** (see SI), also prepared independently (see below).

The corresponding  $\text{CrO}_3$  oxidation of metalloisobacteriochlorin **13M-E** revealed the formation of all three possible isomers, also in overall combined yield of ~60%, but in different ratios than resulting from the CTAP-mediated oxidation of metalloisobacteriochlorin osmate esters **12M-E**. Isomers  $4^{2,8}\text{Pt}$  and  $4^{2,7}\text{Pt}$  were observed as most abundant isomers, in a ratio of 1:1, with only a trace of the  $4^{3,7}$  isomer. An HPLC profile of the fraction of the three isomers of **4Pt** illustrates this (Figure 9A). The separation of the corresponding **4Zn** was also possible but more difficult (see SI).

The UV–vis spectra of all three fractions were recorded (Figure 9B). The differences among the spectra of the regioisomers, including the stark differences in their extinction coefficients (see SI), are remarkable and continue the trend observed for the two regioisomers of bacteriolactones.<sup>4</sup> We will discuss below in more detail the UV–vis spectra of the individual isomers of the corresponding free bases as well as provide some rationalization of the uneven formation of the regioisomers.

**Free Base Isobacteriolactones by One-Step Oxidation of *meso*-( $\text{C}_6\text{F}_5$ )-porphyrin **1**.** Free base porphyrin **1** proved to be susceptible to direct oxidation using a 10-fold stoichiometric excess of CTAP (Scheme 8). This reaction

## Scheme 7. Synthetic Pathways toward Regioisomeric Mixtures of Metalloisobacteriodilactones 4M

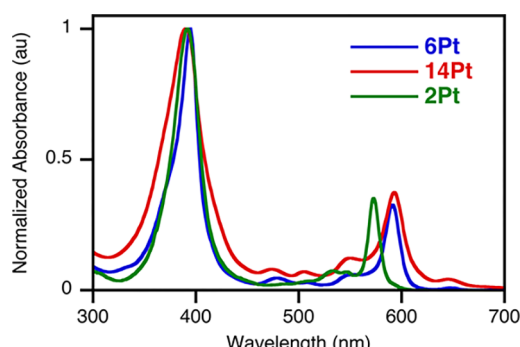
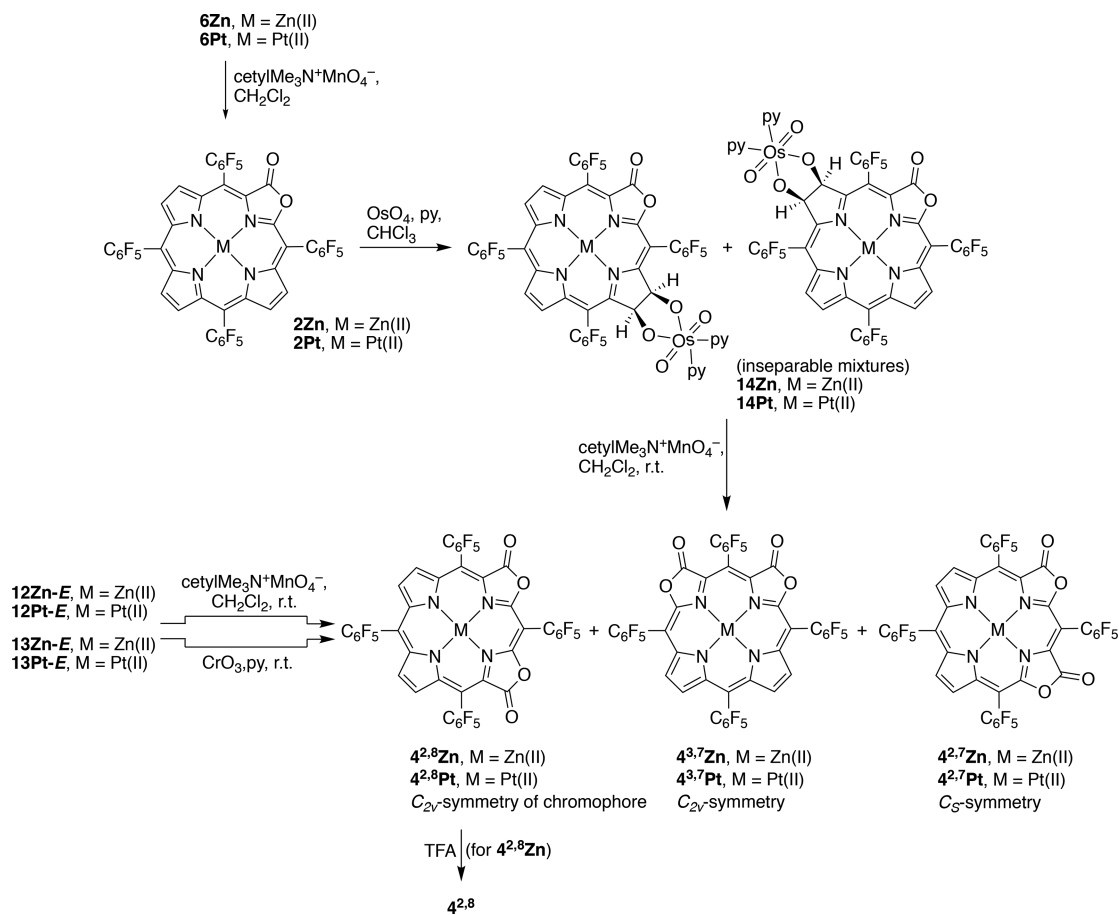


Figure 7. UV-vis absorption spectra ( $\text{CH}_2\text{Cl}_2$ ) of the compounds indicated.

generated a number of products, among them porpholactone **2** (15%) and some hydroxylated products, such as known dihydroxychlorin **5** and dihydroxyisobacteriolactone **15** (both in <5% yield). The identity of **15** could be readily demonstrated by the generation of an identical (by  $R_f$  value, UV-vis spectroscopy, and MS) compound by acid-induced demetallation of **15Zn**. Most significantly in the context of this contribution, a fraction containing all three isobacteriochlorin dilactone isomers **4** (in 25% combined yield) was the main product of this oxidation. All three isomers possessed the identical composition of  $\text{C}_{42}\text{H}_{20}\text{F}_{20}\text{N}_4\text{O}_4$  of their  $[\text{M} - \text{H}^+]$ -ion (as shown by ESI-). Notably, no bacteriochlorin-type derivatives were observed. Thus, the outcome of the direct oxidation of free base *meso*-pentafluorophenylporphyrin **1** is

greatly oxidant-dependent, with Gouterman's conditions ( $\text{Ag}^+$ /oxalate/AcOH,  $\Delta$ ) generating all dilactone isomers,<sup>16</sup> Zhang's conditions ( $\text{RuO}_4$ /bipy/aqueous base/biphasic with  $\text{CH}_2\text{Cl}_2$ ,  $\Delta$ ) generating primarily (or even exclusively) the bacteriodilactones, and CTAP generating exclusively the isobacteriochlorin series.<sup>17</sup> We cannot offer a rationalization for this observation.

The observation of the two alcohols **5** and **15** suggests that they are intermediates in the direct  $\text{MnO}_4^-$ -mediated oxidation of **1**; their small proportion within the reaction mixture fits the observation that they are readily oxidized to the corresponding lactones (vide infra). Because of the known ability of  $\text{MnO}_4^-$  to convert olefins to diols,<sup>37</sup> this reaction outcome is not surprising per se, but the high susceptibility of the two pseudo-olefinic  $\beta, \beta'$ -bonds of the aromatic  $18 + 4 \pi$ -system of the *meso*- $\text{C}_6\text{F}_5$ -substituted porphyrin **1** toward functionalization with  $\text{MnO}_4^-$  is remarkable. Also surprising is that we found that *meso*- $\text{C}_6\text{H}_5$ -substituted porphyrin is essentially inert to the same reaction conditions. Given the proclivity of free base chlorins to form bacteriochlorins upon modification of a second double bond,<sup>33</sup> the absence of any bacteriochlorin-like chromophores was also not expected. However, since certain reductions of porpholactones form regioselectively the isobacteriochlorin-type chromophore (Scheme 5),<sup>32</sup> the observation of **15** might suggest that its precursor is a porpholactone, rather than a tetrahydroxyisobacteriochlorin.

Purely statistically, a 1:2:1 ratio of  $4^{2,8}:4^{2,7}:4^{3,7}$  would be expected to form by oxidation of **1**. However, the three isomers of isobacteriodilactone **4** do not form in a statistical manner.

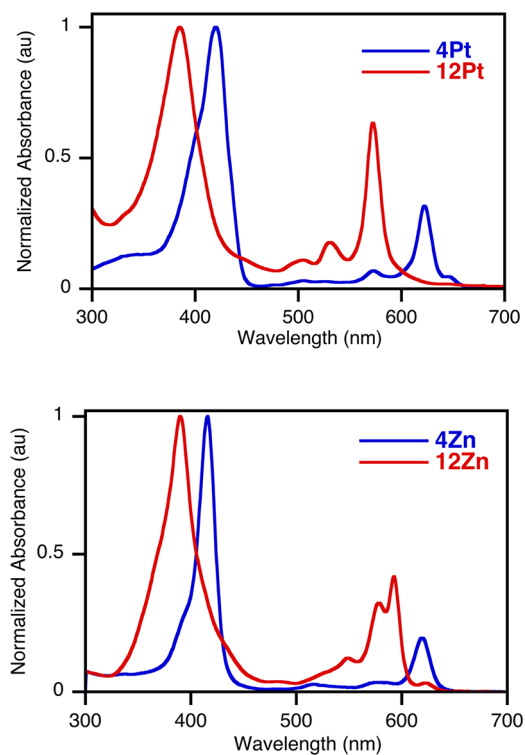


**Figure 8.** UV-vis absorption spectra ( $\text{CH}_2\text{Cl}_2$ ) of the mixture of the three isobacteriochlorindilactones **4M** formed in the CTAP-mediated oxidation of the corresponding isobacteriochlorin tetraol bisosmate ester metal complex **12M-E**.

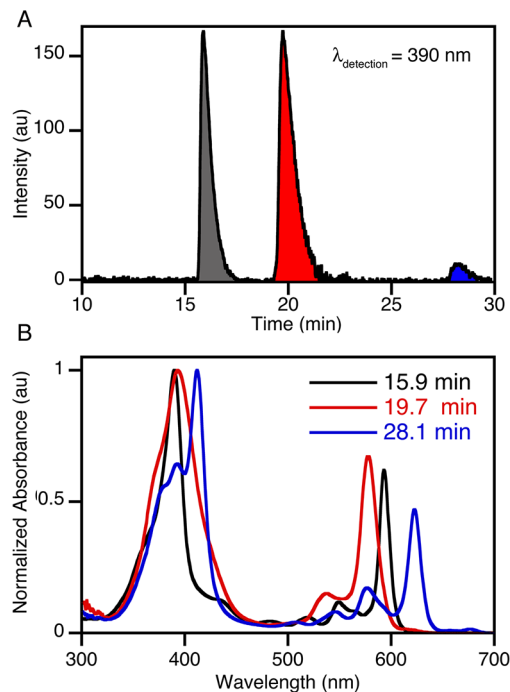


**Figure 9.** (A) HPLC trace (detection  $\lambda$  at 390 nm) of the isobacteriodilactone Pt isomers **4Pt** made by  $\text{CrO}_3$ -mediated oxidation of **13Pt-E**. HPLC conditions: 5  $\mu\text{m}$  silica column (4.6  $\times$  250 mm), isocratic delivery of hexanes and ethyl acetate (99:1 v/v) at a flow rate of 1.5 mL/min. Samples were dissolved in ethyl acetate prior to injection. (B) UV-vis spectra (hexanes/ethyl acetate of 99:1) of the three fractions detectable by HPLC.

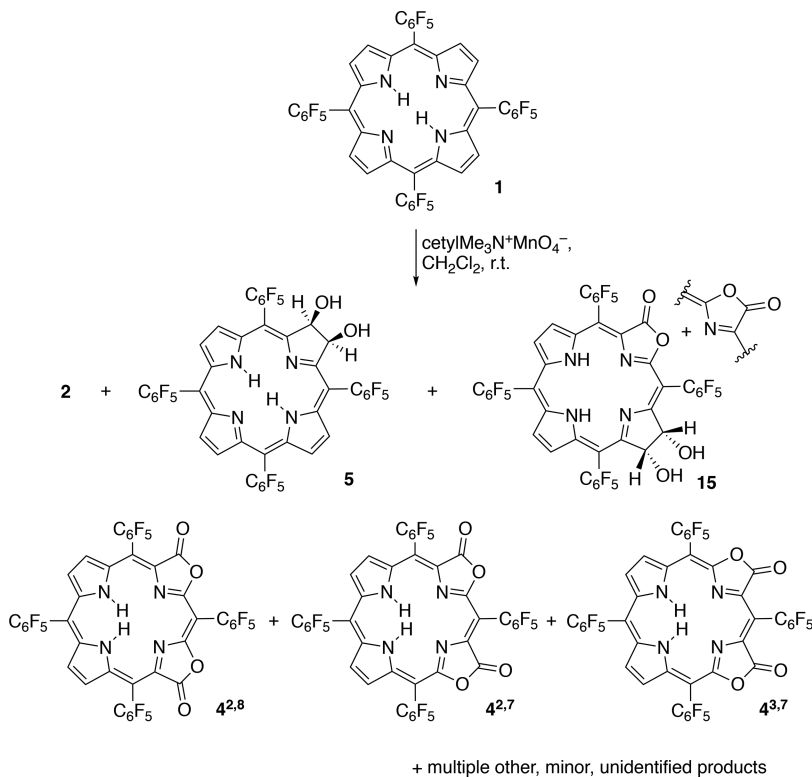
An HPLC analysis of a crude fraction containing all isobacteriodilactones shows them to be present in a 1:1:0.125 ratio (Figure 10A), a finding also confirmed by  $^1\text{H}$  NMR analysis of this mixture (Figure 11). The assignment of the isomers rests on a combination of NMR spectroscopy, computation, and ultimately, the single-crystal structure analysis of two out of the three isomers, detailed below.

Computations quantify the thermodynamic differences between the isomers (Table 1), even though we assume this irreversible oxidation reaction to be kinetically controlled. The bacteriochlorin isomers of the dilactones are relatively more stable than all the isobacteriochlorins, a finding generally attributed to the sterically more demanding arrangement of the two inner NH hydrogen atoms when forced to be located on adjacent rather than opposite nitrogen atoms.<sup>38</sup> The small energy difference between the isobacteriochlorins favoring the  $3^{2,13}$  isomer is commensurate with the observation of an excess of this isomer in the reaction mixture. The most stable isobacteriodilactone is the  $4^{2,8}$  isomer, the isomer found also to be the most prevalent in the product mixture resulting from the  $\text{MnO}_4^-$ -mediated oxidation of **2M** (although the calculations may not directly translate to the metal complexes), and is found in about a 1:1 ratio with the  $4^{2,7}$  isomer in a number of other reactions. The higher than thermodynamically expected occurrence of the  $4^{2,7}$  isomer reflects its higher statistical chance of formation and—most likely—also that the reactions may not be thermodynamically controlled.<sup>33</sup> Be that as it may, the least thermodynamically stable compound is also the least prevalent, and the 2.5 kcal/mol difference to the  $4^{2,8}$  isomer suggests at least an order of magnitude lower occurrence, as is approximately found experimentally, also. The two carbonyl groups of adjacent oxazolidones that point in isomer  $4^{3,7}$  toward the same *meso*-aryl group cause some steric constriction. We posit that this steric effect contributes to the higher energy of this isomer.

Single-pass preparative TLC (silica, 50% hexanes/ $\text{CH}_2\text{Cl}_2$ ) of the isomer mixture enriches the  $4^{2,8}$  (blue solid) and  $4^{2,7}$  (purple solid) isomer fractions to about 90% purity, and the rare isomer  $4^{3,7}$  (green solid) was isolated in 95%+ purity (Figure 11). Both isomers  $4^{2,8}$  and  $4^{3,7}$  are  $C_{2v}$  symmetric, each exhibiting in their  $^1\text{H}$  NMR two doublets (8.71, 8.61 ppm,  $J$  = 5.0 Hz for  $4^{2,8}$  and 8.87, 8.83 ppm,  $J$  = 5.0 Hz for  $4^{3,7}$ ) and a single carbonyl peak (at 164.5 and 164.1 ppm for  $4^{2,8}$  and  $4^{3,7}$ , respectively) in their  $^{13}\text{C}$  NMR spectra. *A priori*, the assignment which of the two  $C_{2v}$  symmetric isomers is which is not readily accomplished, even though the shifts in their  $^1\text{H}$  NMR and  $^{19}\text{F}$  NMR spectra are significantly different. As demonstrated below, their crystal structures and their computed electronic properties allowed their unambiguous identification. The  $C_s$ -symmetric isomer  $4^{2,7}$  is readily identified by its three  $\beta$ -peaks existing as three doublets in 1:1:2 ratio (8.79, 8.68, 8.65 ppm) and two carbonyl peaks appearing in the  $^{13}\text{C}$  NMR at 164.77 and 164.80 ppm.

**Experimental and Computed Optical Spectra of the Isobacteriodilactone Isomers.** The UV-vis spectra of the free-base isobacteriodilactones are all chlorin-like but with split Soret bands and blue-shifted  $\lambda_{\text{max}}$  (Figure 10A) compared to the (more porphyrin-like) spectrum of monolactone **2**.<sup>23</sup> Similar to the bacteriodilactone regioisomers **3**,<sup>4</sup> the isobacteriodilactone regioisomers **4** also all exhibit much different optical properties. Among all three isobacteriodilactones **4**, the  $\lambda_{\text{max}}$  band of isomer  $4^{2,8}$  is the most red-shifted; it is  $\sim$ 10 nm red-shifted ( $\lambda_{\text{max}}$ ) compared to  $4^{2,7}$  and 17 nm red-

Scheme 8



shifted ( $\lambda_{\max}$ ) compared to 4<sup>3,7</sup>. The splitting of the Soret bands in 4<sup>2,8</sup> and 4<sup>2,7</sup> (~20 nm splits) collapses in 4<sup>3,7</sup> into a single band at about an intermediate wavelength between the Soret bands of the other two isomers. The fluorescence emission wavelengths mirror this trend (Figure 10B).

The absorption spectra of the three isobacteriolactones are well reproduced by time-dependent density functional theory (TD-DFT) calculations (Figure 12). The  $\lambda_{\max}$  absorption Q-band was found to possess 65–73% HOMO  $\rightarrow$  LUMO and 26–32% (HOMO–1)  $\rightarrow$  (LUMO+1) character. In line with the four orbital model for isobacteriochlorins, we assign this spectral feature as the Q<sub>y</sub> state. Interestingly, this excitation was predicted to induce very different charge redistributions among the isomeric chromophores. The dipole moment (idealized aligned with the C5–C15 axis) is predicted to decrease by 0.8 D for 4<sup>2,8</sup> and 4<sup>2,7</sup> upon excitation but increases by 1.7 D for 4<sup>3,7</sup> (Table 2) and is associated with a reversal of the electron density flow vector. The reversal in the direction of the ground-to-excited state charge shift is attributable to an energetic inversion of the LUMO and LUMO+1 orbitals, as evidenced from the orbital topologies (Figure 13). The molecular orbitals also highlight to which degree the lactone moiety is in electronic communication with the central 18 $\pi$ -system, as was also the case in other porpholactone derivatives.<sup>23</sup> This also rationalizes the stark differences between the UV–vis spectra of the isobacteriochlorin tetraol 12M-E and any of the isomers of the corresponding metalloisobacteriolactone 4M.

**Crystal Structure Analyses of Isobacteriolactones 4<sup>2,8</sup> and 4<sup>2,7</sup>.** Crystals of isobacteriolactone 4<sup>2,8</sup> and a mixture of the two isobacteriolactones 4<sup>2,8</sup> and 4<sup>2,7</sup> (major component) could be grown that were suitable for analysis by single-crystal X-ray diffractometry. The latter crystal allowed the isolation of the two structures of each component,

ultimately confirming the connectivities of the isomers 4<sup>2,8</sup> and 4<sup>2,7</sup> (Figure 14A,B). Both compounds are moderately distorted from planarity, likely because of (additive) carbonyl-*meso*-aryl group steric interactions that were also derived for the monolactones.<sup>23</sup> The regiosomers show differing deformation modes (Figure 14C): While isomer 4<sup>2,7</sup> is mostly domed and propellered, with some minor waving(x) deformations, isomer 4<sup>2,8</sup> is mostly saddled, with some smaller doming and waving(x) deformations.<sup>42</sup>

## CONCLUSIONS

The stepwise, controlled, and high-yielding preparation of porpholactone isomers via the porphyrin  $\rightarrow$  tetrahydroxybacteriochlorin  $\rightarrow$  bacteriolactone or porphyrin  $\rightarrow$  porpholactone  $\rightarrow$  dihydroxybacteriolactone  $\rightarrow$  bacteriolactone pathways is complementary to those described previously with the added benefit that it generates only the two regiosomeric bacteriochlorins 3, with no need to separate them from any monolactone or other dilactone isomers. Like some of the oxidation methodologies developed by the group of Zhang,<sup>17</sup> these routes are also applicable to the formation of other *meso*-arylporphyrins,<sup>30</sup> although this was not demonstrated here.

Starting from the metalloporphyrins or metalloporpholactones, equivalent strategies ([porphyrin]M  $\rightarrow$  [tetrahydroxyisobacteriochlorin]M  $\rightarrow$  [isobacteriolactone]M or [porphyrin]M  $\rightarrow$  [porpholactone]M  $\rightarrow$  [dihydroxyisobacteriolactone]M  $\rightarrow$  [isobacteriolactone]M) could be developed for the selective generation of the three possible isobacteriolactone isomers 4. Their separation could be achieved. Lastly, a direct oxidation of free base tetrakis-C<sub>6</sub>F<sub>5</sub>-porphyrin to generate a host of known products together with the free base isobacteriolactone isomers 4 was developed. After their first discovery in 1989,<sup>16</sup> this is the first report of

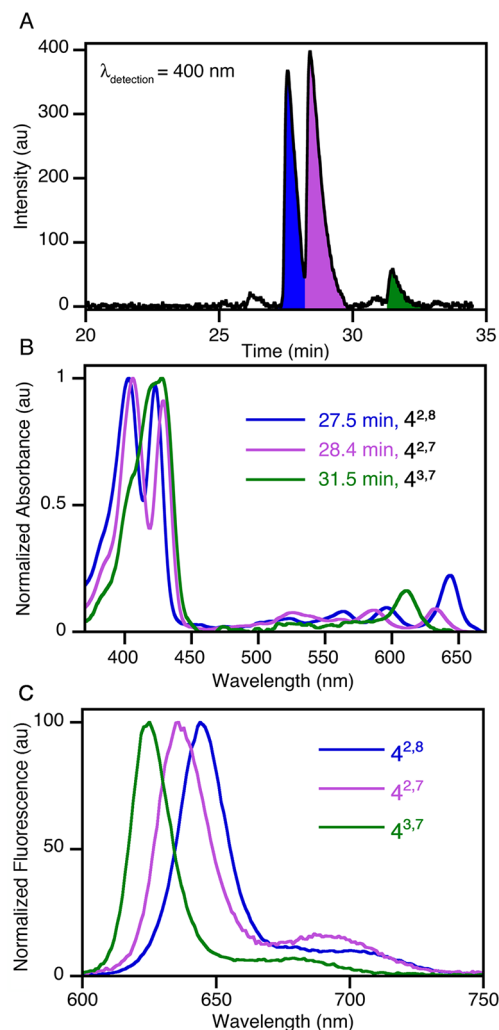


**Figure 10.** (A) HPLC traces (detection  $\lambda$  at 400 nm) of the free base isobacteriochlorindilactone isomer mixture. HPLC conditions: 5  $\mu$ m silica column (4.6  $\times$  250 mm), isocratic delivery of hexanes and ethyl acetate (99:1 v/v) at a flow rate of 1.5 mL/min. Samples were dissolved in ethyl acetate prior to injection. (B) UV-vis absorption (hexanes/ethyl acetate 99:1) and (C) fluorescence emission (hexanes/ethyl acetate 99:1;  $\lambda_{\text{excitation}} = \lambda_{\text{Soret}}$ ) spectra of the isobacteriochlorindilactone isomers 4 indicated.

their rational or efficient syntheses. The three isobacterioliactone isomers  $4^{2,7}$ ,  $4^{3,7}$ , and  $4^{2,8}$  possess significantly varying optical properties. The key to the understanding of this phenomenon was derived computationally. The three isomers possess differing (in one case, inverted) energetic orderings and topologies of their LUMOs, such that the same electronic excitations into their LUMOs produce different dipolar responses.

We thus present rational pathways toward all isomers of the *meso*-tetrakis-C<sub>6</sub>F<sub>5</sub>-derivatized dilactones, making them accessible for further study.

## EXPERIMENTAL SECTION

**Materials.** All solvents and reagents (Aldrich, Acros) were used as received. *meso*-Tetrakis(pentafluorophenyl)porphyrin 1<sup>43</sup> was provided by a commercial supplier. Known metalloporphyrins 1Zn and 1Pt were prepared by metal insertion into 1 using standard methods.<sup>43,44</sup> Analytical (aluminum backed, silica gel 60, 250  $\mu$ m thickness) and preparative (20  $\times$  20 cm, glass backed, silica gel 60,

500  $\mu$ m thickness) TLC plates and standard grade, 60  $\text{\AA}$ , 32–63  $\mu$ m flash column silica gel were used.

**CAUTION:** OsO<sub>4</sub> is a highly toxic, volatile solid that must be handled exclusively under a well-ventilated fume hood. Particular hazards are inhalation and exposure of the eye to OsO<sub>4</sub> fumes. Personal protective equipment (nitrile gloves, lab coat, and safety goggles) are required. Reactions were frequently scaled such that the contents of an entire OsO<sub>4</sub> ampule could be used all at once; the ampule was broken open (leather gloves over the nitrile gloves) and cap and ampule were immediately dumped into the reaction flask containing all other solvents and reactants; the glass was retrieved by filtration or with pincers before the solvent was removed by rotary evaporation. When less than the contents of an entire OsO<sub>4</sub> ampule was required, the OsO<sub>4</sub> was dissolved in distilled pyridine in a volumetric flask, well-sealed, stored cold, and used within days. Wastes that might contain unreacted OsO<sub>4</sub> were treated with NaHSO<sub>3</sub> before disposal.

**Fluorescence Measurements.** The fluorescence quantum yields ( $\phi$ ) were determined relative to that of *meso*-tetraphenylporphyrin 1 (0.13 in CH<sub>2</sub>Cl<sub>2</sub>);<sup>45</sup>  $\lambda_{\text{excitation}} = \lambda_{\text{Soret}}$ .

**Computations.** All structures were optimized with the Becke, three-parameter, Lee–Yang–Parr (B3LYP) hybrid functional, a 6-31g(d) basis set, and an ultrafine grid for integration, as implemented in Gaussian 09 revision D.01.<sup>41</sup> Frequency calculations were performed for each molecule; we confirmed that local minima were obtained. Ground- and excited-state energies and dipole moments, as well as time-dependent density functional theory (TD-DFT) excitation energies, were calculated with the CAM-B3LYP/6-31g(d) model chemistry for the already optimized structures. For further computational details, see the SI.

**X-ray Single-Crystal Diffractometry.** Details of the data collection and structural parameters for the structure elucidation of  $4^{2,7}$ ,  $4^{2,8}$ , 6, 7-Z, 9, and 12Zn-E, including CIF files, descriptions of disorder and hydrogen atom treatment, and software packages used, can be found in the SI.

**General Procedure A: Osmylation of *meso*-Tetrakis(pentafluorophenyl)porphyrin 1, Its Metal Complexes 1M, and Related Compounds.** The porphyrin was dissolved in a round-bottom flask equipped with a stir bar in CHCl<sub>3</sub> and freshly distilled pyridine. The mixture was treated with OsO<sub>4</sub> (stock solution made of 1.0 g OsO<sub>4</sub> dissolved in 50 mL of pyridine). The flask was stoppered, shielded from light with aluminum foil, and stirred at ambient temperature. The disappearance of the starting material/appearance of the product was monitored by TLC and UV-vis spectroscopy. Once no further progress of the reaction was detectable (after  $\sim$ 24 h), the solvent was removed to dryness by rotary evaporation, and the crude mixture was separated by column chromatography (silica–CH<sub>2</sub>Cl<sub>2</sub>/1.0% MeOH).

**General Procedure B: Reductive Cleavage of Chlorin Diol Osmate Esters.** Once the osmylation reaction as described above was complete (TLC control), approximately 50% of the solvent was removed by rotary evaporation. To the crude reaction mixture was added a saturated solution of NaHSO<sub>3</sub> in MeOH/H<sub>2</sub>O (1:1). The flask was stoppered and wrapped in aluminum foil, and the biphasic solution was vigorously stirred at ambient temperature for 2 d. Once no further progress of the reaction was detectable by TLC, the mixture was transferred into a separatory funnel. After the addition of CH<sub>2</sub>Cl<sub>2</sub> ( $\sim$ 50 mL), the organic fraction was separated and filtered through a short plug of diatomaceous earth (Celite). The solvent was then removed to dryness by rotary evaporation. A gentle stream of N<sub>2</sub> for several hours ensured that the crude material was thoroughly dried before it was purified via flash chromatography (silica cartridge–CH<sub>2</sub>Cl<sub>2</sub>/1.0% MeOH).

**General Procedure C: CTAP-Mediated Oxidative Cleavage of Chlorin Osmate Esters To Provide Corresponding Lactones.** Chlorin diol osmate ester (6) was dissolved in a round-bottom flask equipped with a stir bar in CH<sub>2</sub>Cl<sub>2</sub>. The mixture was treated with cetyltrimethylammonium MnO<sub>4</sub> (CTAP). The flask was stoppered, shielded from light with aluminum foil, and stirred at ambient temperature. The disappearance of the starting material/appearance

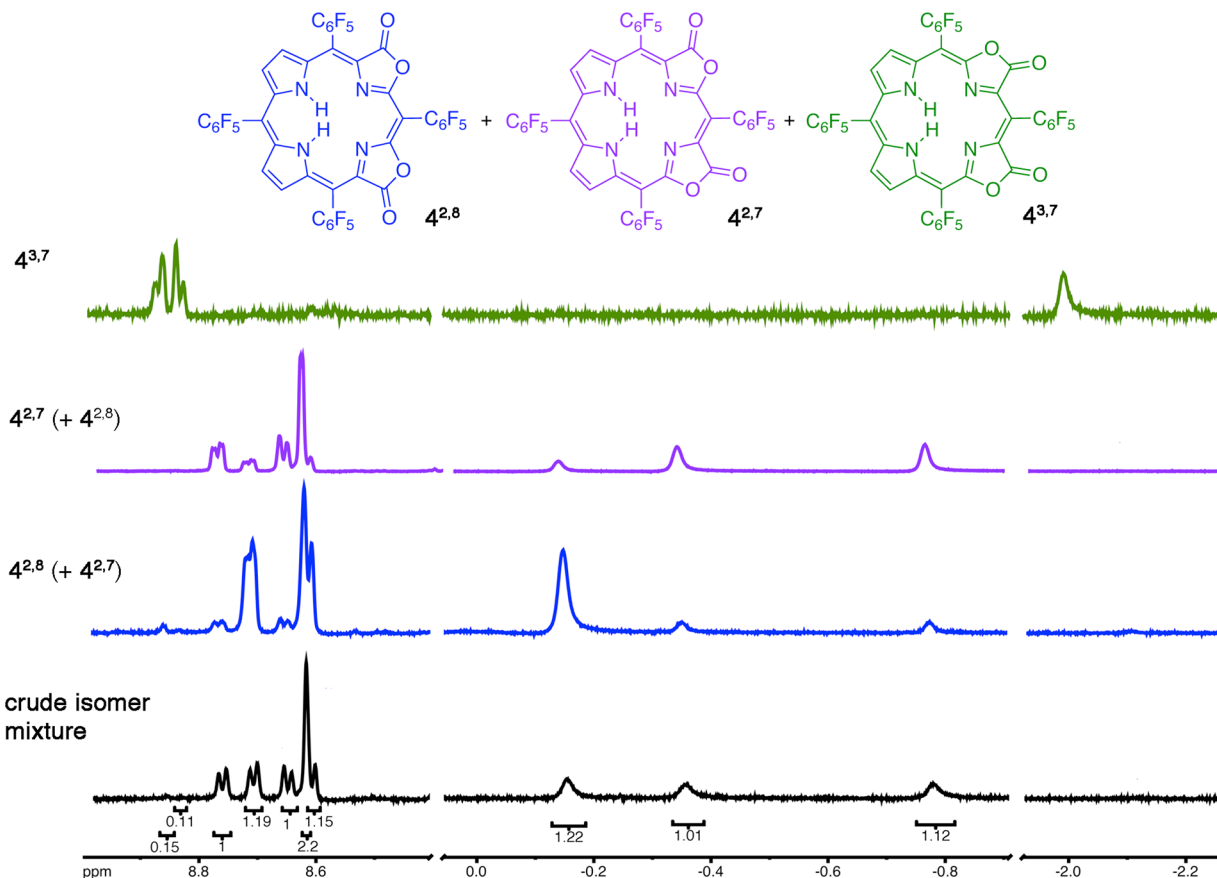


**Figure 11.**  $^1\text{H}$  NMR spectra (400 MHz,  $\text{CDCl}_3$ , 25 °C) of a crude fraction of the three isobacteriodilactones **4** and the spectra of the enriched/separated isomers indicated.

**Table 1. Computed Relative Stability of All Dilactone Isomers<sup>a</sup>**

compound	relative stability, kcal/mol (kJ/mol)
<b>3<sup>2,13</sup></b>	0.0 (0.0)
<b>3<sup>2,12</sup></b>	0.6 (2.5)
<b>4<sup>2,8</sup></b>	6.1 (25.6)
<b>4<sup>2,7</sup></b>	7.1 (29.8)
<b>4<sup>3,7</sup></b>	8.6 (36.1)

<sup>a</sup>Calculated using the B3LYP-D3/6-31g(d) model chemistry<sup>39</sup> with  $\text{CH}_2\text{Cl}_2$  solvation via the conductor-like polarizable continuum model.<sup>40</sup>

of the product was monitored by TLC. Upon consumption of the starting material (~30 min), the reaction mixture was filtered through a short silica plug, and the filter cake was washed with  $\text{CH}_2\text{Cl}_2$  until the product was completely removed from the plug. The filtrate was then condensed under vacuum and purified via flash chromatography (silica–50% hexanes/ $\text{CH}_2\text{Cl}_2$ ).

**General Procedure D:  $\text{CrO}_3$ -Mediated Oxidative Cleavage of Chlorin Diols To Provide the Corresponding Lactones.** Chlorin diols (**5**) were dissolved in pyridine in a round-bottom flask equipped with a stir bar. The mixture was treated with  $\text{CrO}_3$ . The flask was stoppered, shielded from light with aluminum foil, and stirred at ambient temperature. The disappearance of the starting material and appearance of the product were monitored by TLC. Once no further progress of the reaction was detectable (after ~30 min), the organic phase was separated and filtered through a short plug of silica. The solvent was removed to dryness by rotary evaporation. A gentle stream of  $\text{N}_2$  for several hours ensured that the crude material was thoroughly dried. The crude material was purified by flash chromatography (silica,  $\text{CH}_2\text{Cl}_2$ /25% hexanes).

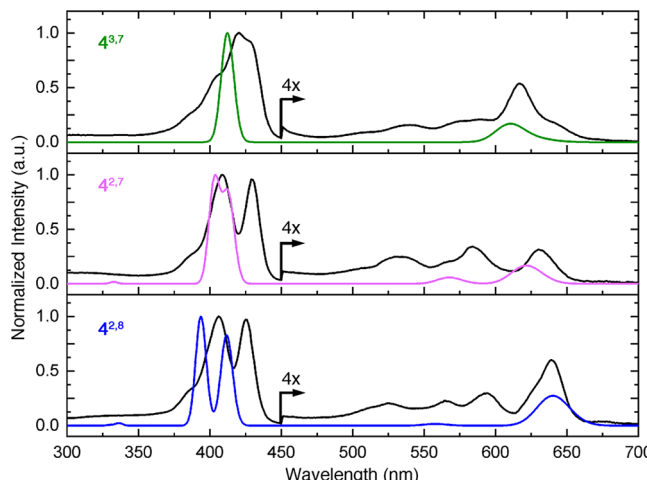


**Figure 12.** Experimental (black) and simulated (colored) spectra for the three isomeric isobacteriodilactones indicated. The simulated curves are based on TD-CAMB3LYP/6-31+g(d) calculations. The calculated wavelengths were systematically red-shifted by 64 nm for better comparison to experiment, and Gaussians having a full width at half-maximum of 0.1 eV were fit to the calculated spectral data.

**meso-Tetrakis(pentafluorophenyl)-2,3-cis-dihydroxychlorin Osmate Ester (6).** Compound **6** was prepared according to general procedure A using *meso*-( $\text{C}_6\text{F}_5$ )-porphyrin **1** (1.00 g,  $1.03 \times 10^{-3}$  mol) and 1 equiv of  $\text{OsO}_4$  ( $1.03 \times 10^{-3}$  mol) in  $\text{CHCl}_3$  (125 mL) and pyridine (25 mL) in a 250 mL round-bottom flask. The compound was isolated as a green-colored solid in ~60% yield (~850 mg). About 10–20% (100–200 mg) of the starting material **1** was

**Table 2.** Relative Ground and Excited-State Energies, Absolute Dipole Moments, and Excitation Wavelengths<sup>a</sup>

isomer	$\Delta E_{gs}^b$ (kcal/mol)	$ \mu_{gs} $ (D)	$ \mu_{es} $ (D)	calcd $\lambda$ (nm) <sup>d</sup>	exp $\lambda$ (nm)
4 <sup>2,8</sup>	0.0	9.07	8.22	640	639
4 <sup>2,7</sup>	0.7	9.88	9.12	621	631
4 <sup>3,7</sup>	2.9	10.77	12.46	610	618

<sup>a</sup>Dipole moments and excitation wavelengths calculated with DFT and TD-DFT, respectively, using the CAM-B3LYP/6-31+g(d) model chemistry. The structures were optimized using B3LYP/6-31g(d)<sup>41</sup> and have hydrogens in place of *meso*-C<sub>6</sub>F<sub>5</sub> substituents. <sup>b</sup>gs = ground state. <sup>c</sup>es = excited state. <sup>d</sup>Red-shifted by 64 nm.

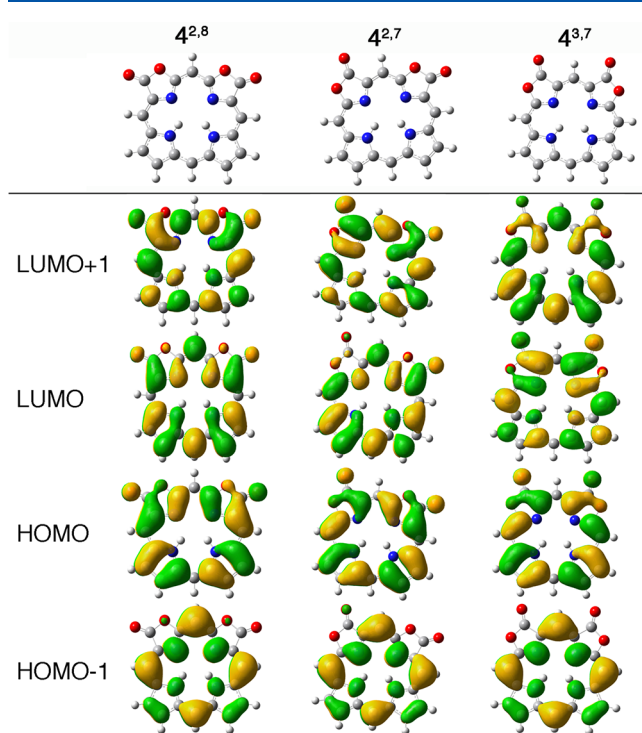


**Figure 13.** Topological evolution of the frontier orbitals of the isobacteriobacteriolactones as derived from DFT calculations. All orbitals are shown at an isosurface value of 0.02 au.

recovered; small and varying amounts (<50 mg) of the corresponding bacteriochlorin tetraol bisosmate ester 7 could also be retrieved from the column. **6:**  $R_f = 0.13$  (silica, CHCl<sub>3</sub>); <sup>1</sup>H NMR (400 MHz, CDCl<sub>3</sub>,  $\delta$ ) 8.75 (d,  $^3J = 4.9$  Hz, 2H), 8.56 (overlapping d,  $^3J = 5.8$  Hz, 4H), 8.55 (overlapping s, 2H), 8.50 (d,  $^3J = 4.9$  Hz, 2H), 7.86 (t,  $^3J = 7.5$ , 7.5 Hz, 2H), 7.40 (t,  $^3J = 6.8$ , 6.9 Hz, 4H), 7.00 (s, 2H), -1.98 (br s, 2H) ppm; <sup>13</sup>C{<sup>1</sup>H} NMR (101 MHz, CDCl<sub>3</sub>,  $\delta$ ) 166.1, 152.8, 149.9, 149.6, 140.7, 140.5, 136.2, 135.5, 132.4, 127.6, 125.2, 124.2, 123.9, 105.3, 98.9, 95.5 ppm; <sup>19</sup>F NMR (376 MHz; CDCl<sub>3</sub>,  $\delta$ ) -134.2 (dd,  $^3J = 24.3$ , 7.7 Hz, 1F), -136.9 (dd,  $^3J = 24.9$ , 8.5 Hz, 2F), -139.2 (dd,  $^3J = 24.3$ , 7.6 Hz, 1F), -152.1 (t,  $^3J = 20.9$  Hz, 1F), -153.9 (t,  $^3J = 20.9$  Hz, 1F), -161.8 (td,  $^3J = 22.3$ , 7.5 Hz, 1F), -162.4 (td,  $^3J = 22.6$ , 6.8 Hz, 1F), -164.2 (td,  $^3J = 22.6$ , 6.9 Hz, 1F) ppm; UV-vis (CH<sub>2</sub>Cl<sub>2</sub>)  $\lambda_{max}$  nm (rel intensity) 408 (1.00), 504 (0.11), 595 (0.03), 647 (0.20), 714 (0.03); fluorescence emission ( $\lambda_{excitation} = \lambda_{Soret}$ ) (CH<sub>2</sub>Cl<sub>2</sub>)  $\lambda_{max}$  650 nm; like all hydrophorphyrin osmate esters, no molecular peak could be detected in the ESI+ or ESI- MS (100% CH<sub>3</sub>CN, 5–30 V cone voltage).

*meso*-Tetrakis(pentafluorophenyl)-2,3-cis-12,13-cis-tetrahydroxybacteriochlorin Osmate Esters (**7-Z** and **-E**). The compounds were prepared by the osmylation of *meso*-(C<sub>6</sub>F<sub>5</sub>)-porphyrin **1** (1.00 g, 1.03  $\times 10^{-3}$  mol) according to the general procedure A using 2 equiv of OsO<sub>4</sub> (0.52 g, 2.06  $\times 10^{-3}$  mol) in CHCl<sub>3</sub> (125 mL) and pyridine (25

mL). The mixture of **7-Z** and **7-E** was isolated as a green-colored, fluffy solid in ~60% yield (~100 mg). **7:**  $R_f = 0.15$  (silica, CHCl<sub>3</sub>); <sup>1</sup>H NMR (400 MHz, CDCl<sub>3</sub>, nonpolar (major) *E*-isomer,  $\delta$ ) 8.53 (d,  $^3J = 5.4$  Hz, 2H), 8.23 (d,  $^4J = 1.7$  Hz, 1H), 7.78 (t,  $^3J = 7.5$ , 7.5 Hz, 1H), 7.33 (t,  $^3J = 7.8$ , 7.8 Hz, 2H), 6.82 (s, 1H), -1.90 (s, 1H) ppm; <sup>13</sup>C{<sup>1</sup>H} NMR (101 MHz, CDCl<sub>3</sub>,  $\delta$ ) 161.6, 149.5, 140.4, 136.6, 130.9, 128.8, 124.9, 122.5, 100.2, 95.2 ppm; <sup>19</sup>F NMR (376 MHz; CDCl<sub>3</sub>,  $\delta$ ) -134.3 (dd,  $^3J = 24.35$ , 7.59 Hz, 1F), -139.5 (dd,  $^3J = 24.44$ , 7.61 Hz, 1F), -154.6 (t,  $^3J = 20.94$  Hz, 1F), -162.8 (td,  $^3J = 22.70$ , 6.91 Hz, 1F), -164.5 (td,  $^3J = 22.64$ , 6.66 Hz, 1F) ppm; UV-vis (CH<sub>2</sub>Cl<sub>2</sub>)  $\lambda_{max}$  nm 354 (0.79), 378 (1.00), 448 (0.08), 479 (0.08), 508 (0.43), 654 (0.05), 715 (0.74); no molecular peak could be detected in the ESI+ or ESI- MS (100% CH<sub>3</sub>CN, 5–30 V cone voltage).

*meso*-Tetrakis(pentafluorophenyl)-2,3-cis-dihydroxychlorinatoZn(II) Osmate Ester (**6Zn**). Prepared according to the general procedure A from **1Zn** (1.00 g, 0.94  $\times 10^{-3}$  mol) using 1 equiv of OsO<sub>4</sub> (0.24 g, 0.94  $\times 10^{-3}$  mol) in CHCl<sub>3</sub> (125 mL) and pyridine (25 mL) and isolated as purple crystals in ~60% yield (~870 mg).  $R_f = 0.3$  (silica, CHCl<sub>3</sub>); <sup>1</sup>H NMR (400 MHz, CDCl<sub>3</sub>,  $\delta$ ) 8.55 (overlapping d,  $^3J = 4.6$  Hz, 1H and m, 2H), 8.47 (s, 1H), 8.25 (d,  $^3J = 4.7$  Hz, 1H), 7.87 (t,  $^3J = 7.4$ , 7.2 Hz, 1H), 7.41 (t,  $^3J = 6.5$ , 6.5 Hz, 2H), 6.87 (s, 1H) ppm; <sup>19</sup>F NMR (376 MHz; CDCl<sub>3</sub>,  $\delta$ ) -134.4 (s, 1F), -137.4 (s, 2F), -139.5 (s, 1F), -153.4 (t,  $^3J = 20.8$  Hz, 1F), -155.3 (s, 1F), -162.4 to -162.7 (m, 2F), -163.0 (s, 1F), -164.9 (s, 1F) ppm; <sup>13</sup>C{<sup>1</sup>H} NMR (101 MHz, CDCl<sub>3</sub>,  $\delta$ ) 161.6, 153.8, 149.4, 146.9, 146.5, 144.3, 140.5, 136.3, 131.7, 128.4, 127.5, 125.0, 122.7, 106.4, 97.4, 95.0 ppm; UV-vis (CH<sub>2</sub>Cl<sub>2</sub>)  $\lambda_{max}$  nm (rel intensity) 415 (1.00), 515 (0.03), 575 (0.03), 618 (0.19); no molecular peak could be detected in the ESI+ or ESI- MS (100% CH<sub>3</sub>CN, 5–30 V cone voltage).

*meso*-Tetrakis(pentafluorophenyl)-2,3-cis-dihydroxychlorinatoplatinum(II) Osmate Ester (**6Pt**). Prepared according to the general procedure A from **1Pt** (1.00 g, 0.92  $\times 10^{-3}$  mol) and 1 equiv of OsO<sub>4</sub> (0.23 g, 0.92  $\times 10^{-3}$  mol) in CHCl<sub>3</sub> (125 mL) and pyridine (25 mL). The product was isolated as a burgundy solid in 50% yield (790 mg). **6Pt:**  $R_f = 0.25$  (silica, CHCl<sub>3</sub>); <sup>1</sup>H NMR (400 MHz, CDCl<sub>3</sub>,  $\delta$ ) 8.52 to 8.46 (m, 4H), 8.28 (d,  $^3J = 4.9$  Hz, 1H), 7.80 (t,  $^3J = 7.5$  Hz, 1H), 7.34 (t,  $^3J = 8.7$ , 2H), 6.90 (s, 1H) ppm; <sup>13</sup>C{<sup>1</sup>H} NMR (101 MHz, CDCl<sub>3</sub>,  $\delta$ ) 154.0, 149.6, 146.0, 140.8, 137.4, 136.2, 132.0, 127.1, 126.2, 125.2, 109.2, 99.9, 93.7 ppm; UV-vis (CH<sub>2</sub>Cl<sub>2</sub>)  $\lambda_{max}$  nm (rel intensity) 395 (1.00), 479 (0.05), 548 (0.06), 591 (0.34); no molecular peak could be detected in the ESI+ or ESI- MS (100% CH<sub>3</sub>CN, 5–30 V cone voltage).

*meso*-Tetrakis(pentafluorophenyl)-2,3-cis-7,8-cis-tetrahydroxyisobacteriochlorinatozinc(II) Osmate Ester *E*-Isomer (**12Zn-E**). Compound **12Zn-E** was prepared according to the general procedure A from **1Zn** (1.00 g, 0.94  $\times 10^{-3}$  mol) using 2 equiv of OsO<sub>4</sub> (0.48 g, 1.88  $\times 10^{-3}$  mol) in CHCl<sub>3</sub> (125 mL) and pyridine (25 mL) and isolated as a green solid in ~60% yield (~1.050 g). **12Zn-E:**  $R_f = 0.25$  (silica, CHCl<sub>3</sub>); <sup>1</sup>H NMR (400 MHz, CDCl<sub>3</sub>,  $\delta$ ) 8.57 (overlapping d,  $^3J = 4.9$  Hz, 2H), 7.89 (d,  $^3J = 4.4$  Hz, 1H), 7.95 to 7.84 (m, 2H), 7.49 (d,  $^3J = 4.3$  Hz, 1H), 7.46 (t,  $^3J = 6.3$  Hz, 2H), 7.39 (t,  $^3J = 6.5$ , 2H), 6.36 (d,  $J = 6.8$  Hz, 1H), 6.32 (d,  $J = 6.8$  Hz, 1H) ppm; <sup>19</sup>F NMR (376 MHz; CDCl<sub>3</sub>,  $\delta$ ) -134.6 (dd,  $^3J = 24.72$ , 7.38 Hz, 2F), -137.2 (dd,  $^3J = 24.74$ , 5.98 Hz, 2F), -138.3 (dd,  $^3J = 24.06$ , 7.85 Hz, 2F), -140.5 (dd,  $^3J = 24.83$ , 7.42 Hz, 2F), -154.5 (t,  $^3J = 20.81$  Hz, 1F), -156.1 (t,  $^3J = 21.00$  Hz, 2F), -157.1 (t,  $^3J = 21.09$  Hz, 1F), -162.9 (td,  $^3J = 22.56$ , 6.70 Hz, 2F), -163.6 (td,  $^3J = 22.56$ , 6.70 Hz, 2F), -164.9 (td,  $^3J = 31.26$ , 14.50 Hz, 2F), -165.2 (td,  $^3J = 31.26$ , 14.50 Hz, 2F) ppm; <sup>13</sup>C{<sup>1</sup>H} NMR (100 MHz, CDCl<sub>3</sub>,  $\delta$ ) 166.9, 157.1, 151.7, 149.5, 149.4, 142.2, 140.5, 128.5, 125.1, 125.1, 122.1, 111.6, 98.8, 94.9, 92.9 ppm; UV-vis (CH<sub>2</sub>Cl<sub>2</sub>)  $\lambda_{max}$  nm (log  $\epsilon$ ) 410 (4.79), 560 (3.85), 605 (4.39); no molecular peak could be detected in the ESI+ or ESI- MS (100% CH<sub>3</sub>CN, 5–30 V cone voltage).

*meso*-Tetrakis(pentafluorophenyl)-2,3-cis-7,8-cis-tetrahydroxyisobacteriochlorinatozinc(II) *E*-Isomer (**13Zn-E**). Compound **13Zn-E** was prepared according to the general procedure B by the cleavage of osmate ester **12Zn-E** (1.54 g, 1.0  $\times 10^{-3}$  mol)

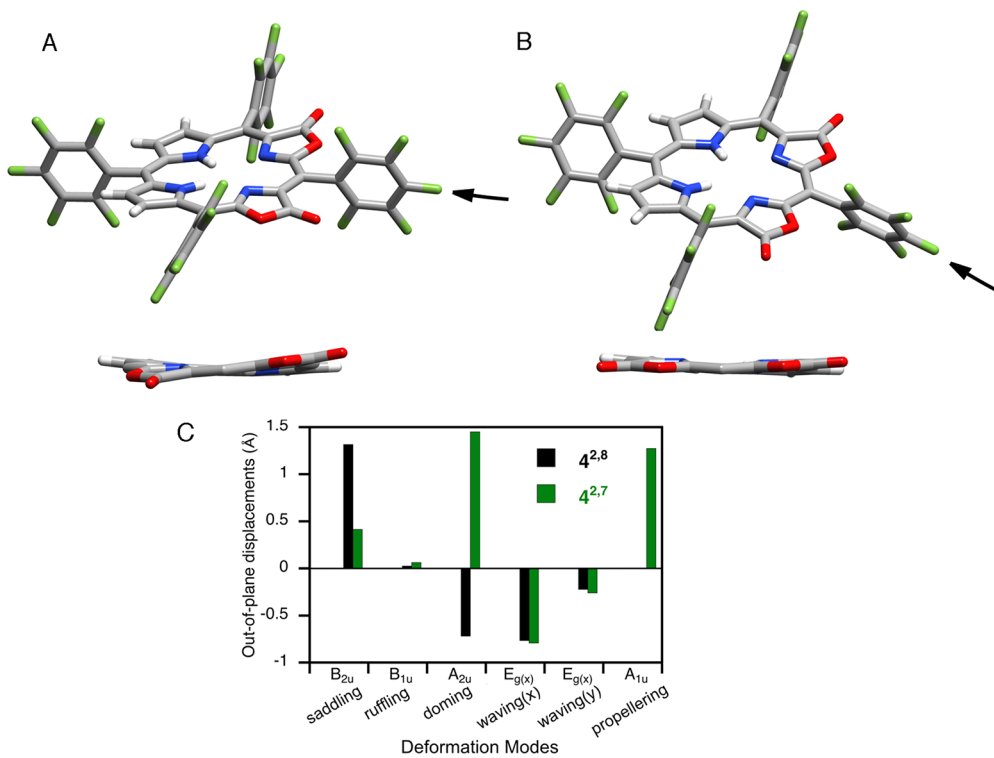


**Figure 14.** Stick representations of the X-ray single-crystal structures of (A) dilactone 4<sup>2,7</sup>, the majority compound of a mixed crystal of 4<sup>2,7</sup> and 4<sup>2,8</sup>, and (B) dilactone 4<sup>2,8</sup>; oblique and side views; the arrow in each oblique view indicates the view direction of the side views. All disorder and solvents removed for clarity. The *meso*-aryl substituents were removed in the side views for clarity. (C) NSD analysis<sup>42</sup> of the independent molecules in the unit cell indicated.

using MeOH/H<sub>2</sub>O (1:1) (80 mL). The product 13Zn-**E** was isolated as a green color solid in ~80% isolated yield (~880 mg). 13Zn-**E**: *R*<sub>f</sub> = 0.22 (silica, 2% CH<sub>3</sub>OH/CH<sub>2</sub>Cl<sub>2</sub>); <sup>1</sup>H NMR (400 MHz, CDCl<sub>3</sub>,  $\delta$ ) 7.89 (d, *J* = 4.2 Hz, 1H), 7.49 (d, *J* = 4.3 Hz, 1H), 5.58 (d, *J* = 7.1 Hz, 1H), 5.54 (d, *J* = 6.9 Hz, 1H) ppm; <sup>19</sup>F NMR (376 MHz; CDCl<sub>3</sub>,  $\delta$ ) –136.3 (d, *J* = 21.67 Hz, 2F), –138.3 (d, *J* = 18.4 Hz, 2F), –138.6 (d, *J* = 17.10 Hz, 2F), –140.5 (d, *J* = 19.83 Hz, 2F), –153.1 (t, *J* = 20.80 Hz, 1F), –153.86 (t, *J* = 23.34 Hz, 2F), –154.02 (t, *J* = 21.06 Hz, 1F), –161.98 to –162.55 (m, 8F) ppm; UV-vis (CH<sub>2</sub>Cl<sub>2</sub>)  $\lambda_{\text{max}}$  nm (rel intensity) 407.4 (1.00), 533.7 (0.09), 596.3 (0.29); fluorescence emission ( $\lambda_{\text{excitation}} = \lambda_{\text{Soret}}$ ) (CH<sub>2</sub>Cl<sub>2</sub>)  $\lambda_{\text{max}}$  600 nm; HR-MS (ESI+, 100% CH<sub>3</sub>CN, TOF) calcd for C<sub>44</sub>H<sub>12</sub>F<sub>20</sub>N<sub>4</sub>O<sub>4</sub>Zn [M]<sup>+</sup> 1103.9825, found 1103.9838.

*[meso-Tetrakis(pentafluorophenyl)-2,3-cis-7,8-cis-tetrahydroxyisobacteriochlorinato]platinum(II) Osmate Esters E-Isomer (12Pt-E).* Compound 12Pt-E was prepared according to the general procedure A from 1Pt (1.00g, 0.92  $\times$  10<sup>-3</sup> mol) and 2 equiv of OsO<sub>4</sub> (0.47 g, 1.84  $\times$  10<sup>-3</sup> mol) in CHCl<sub>3</sub> (125 mL) and pyridine (25 mL). The product was isolated as a red solid in ~60% isolated yield (~1.10 g). 12Pt-E: *R*<sub>f</sub> = 0.20 (silica, CHCl<sub>3</sub>); <sup>1</sup>H NMR (400 MHz, CDCl<sub>3</sub>,  $\delta$ ) 8.58 (d, <sup>3</sup>J = 5.0 Hz, 2H), 8.55 (d, <sup>3</sup>J = 5.0 Hz, 2H), 8.01 (d, <sup>3</sup>J = 4.2 Hz, 1H), 7.88 to 7.75 (m, 2H), 7.71 (d, <sup>3</sup>J = 4.2 Hz, 1H), 7.43 (t, <sup>3</sup>J = 6.5 Hz, 2H), 7.36 (t, <sup>3</sup>J = 6.5 Hz, 2H), 6.48 (d, <sup>3</sup>J = 7.0 Hz, 1H), 6.44 (d, <sup>3</sup>J = 7.0 Hz, 1H) ppm; <sup>19</sup>F NMR (376 MHz; CDCl<sub>3</sub>,  $\delta$ ) –133.9 (dd, <sup>3</sup>J = 24.02, 7.27 Hz, 2F), –136.6 (dd, <sup>3</sup>J = 24.42, 6.83 Hz, 2F), –137.6 (dd, <sup>3</sup>J = 23.34, 7.72 Hz, 2F), –139.8 (dd, <sup>3</sup>J = 24.36, 7.47 Hz, 2F), –153.1 (t, <sup>3</sup>J = 20.92 Hz, 1F), –154.8 (t, <sup>3</sup>J = 20.97 Hz, 2F), –155.8 (t, <sup>3</sup>J = 21.11 Hz, 1F), –161.9 (td, <sup>3</sup>J = 22.00, 6.58 Hz, 2F), –162.8 (td, <sup>3</sup>J = 22.57, 6.89 Hz, 2F), –164.0 (td, <sup>3</sup>J = 22.56, 7.12 Hz, 2F), –164.6 (td, <sup>3</sup>J = 22.56, 7.12 Hz, 2F) ppm; <sup>13</sup>C{<sup>1</sup>H} NMR (101 MHz, CDCl<sub>3</sub>,  $\delta$ ) 159.6, 149.6, 149.5, 148.3, 142.6, 140.6, 131.6, 127.4, 125.2, 125.1, 120.4, 113.2, 100.4, 96.5, 93.6, 92.1 ppm; UV-vis (CH<sub>2</sub>Cl<sub>2</sub>)  $\lambda_{\text{max}}$  nm (log  $\epsilon$ ) 384 (4.80), 506 (3.83), 529 (4.08), 573 (4.67), 699 (3.06); IR (KBr)  $\nu_{\text{max}}$  1766 cm<sup>–1</sup>. No molecular peak could be detected in the ESI+ or ESI– MS (100% CH<sub>3</sub>CN, 5–30 V cone voltage).

*[meso-Tetrakis(pentafluorophenyl)-2,3-cis-7,8-cis-tetrahydroxyisobacteriochlorinato]platinum(II) (13Pt-E).* compound 13Pt-E was prepared according to the general procedure B by the cleavage of osmate ester 12Pt-E (1.25g, 1.0  $\times$  10<sup>-3</sup> mol) using MeOH:H<sub>2</sub>O (1:1) (80 mL). The product was isolated as a red-colored solid in ~80% yield (~980 mg). 13Pt-E: *R*<sub>f</sub> = 0.33 (silica, 2% CH<sub>3</sub>OH/CH<sub>2</sub>Cl<sub>2</sub>); <sup>1</sup>H NMR (400 MHz; 2% CD<sub>3</sub>OD/CDCl<sub>3</sub>,  $\delta$ ) 7.98 (d, *J* = 4.5 Hz, 1H), 7.73 (d, *J* = 4.7 Hz, 1H), 5.63 (d, *J* = 7.1 Hz, 1H), 5.57 (d, *J* = 7.3 Hz, 1H) ppm; <sup>19</sup>F NMR (376 MHz; 2% CD<sub>3</sub>OD/CDCl<sub>3</sub>,  $\delta$ ) –135.8 (dd, *J* = 23.67, 7.17 Hz, 2F), –138.1 (dd, *J* = 23.13, 7.1 Hz, 4F), –140.6 (dd, *J* = 23.84, 6.90 Hz, 2F), –152.6 (t, *J* = 20.82 Hz, 1F), –154.1 (t, *J* = 20.71 Hz, 2F), –154.8 (t, *J* = 20.62 Hz, 1F), –161.7 (dt, *J* = 21.48, 6.45 Hz, 2F), –162.7 (dt, *J* = 21.82, 11.08 Hz, 4F), –163.4 (dt, *J* = 22.31, 6.15 Hz, 2F) ppm; UV-vis (CH<sub>2</sub>Cl<sub>2</sub>)  $\lambda_{\text{max}}$  nm (rel intensity) 376.0 (1.00), 507.4 (0.20), 565.7 (0.60); HR-MS (ESI+, 100% CH<sub>3</sub>CN, TOF) calcd for C<sub>44</sub>H<sub>12</sub>F<sub>20</sub>N<sub>4</sub>O<sub>4</sub>Pt [M]<sup>+</sup> 1235.0182, found 1235.0198.

*[meso-Tetrakis(pentafluorophenyl)-2-oxa-3-oxoporphyrin (2).* Compound 2 was prepared according to the general procedure C from 6 (25.0 mg, 0.02  $\times$  10<sup>-3</sup> mol) using ~6 equiv of CTAP (60 mg, 0.12  $\times$  10<sup>-3</sup> mol) in CH<sub>2</sub>Cl<sub>2</sub> (20 mL). The product 2 was isolated as a purple solid in ~50% yield (~10 mg). Spectroscopic properties are identical to those reported previously.<sup>23</sup>

*[meso-Tetrakis(pentafluorophenyl)-2-oxa-3-oxoporphyrinato-zinc(II) (2Zn).* Compound 2Zn was prepared according to the general procedure C from 6Zn (25 mg, 0.02  $\times$  10<sup>-3</sup> mol) using ~6 equiv of CTAP (60 mg, 0.12  $\times$  10<sup>-3</sup> mol) in CH<sub>2</sub>Cl<sub>2</sub> (20 mL). The product 2Zn was isolated as a blue solid in ~50% isolated yield (~11 mg). Spectroscopic properties are identical to those reported previously.<sup>35</sup>

*[meso-Tetrakis(pentafluorophenyl)-2-oxa-3-oxoporphyrinato-platinum(III) (2Pt).* Compound 2Pt was prepared according to the general procedure C from 6Pt (30 mg, 0.02  $\times$  10<sup>-3</sup> mol) using ~6 equiv of CTAP (60 mg, 0.12  $\times$  10<sup>-3</sup> mol). The product 2Pt was isolated as a burgundy-colored solid in ~50% yield (~12 mg). Spectroscopic properties are identical to those reported previously.<sup>35</sup>

**meso-Tetrakis(pentafluorophenyl)-2,3-cis-dihydroxy-12-oxa-13-oxochlorin Osmate Ester (9).** Compound 9 was prepared according to the general procedure A from 2 (100 mg,  $0.10 \times 10^{-3}$  mol) and 1 equiv of  $\text{OsO}_4$  (0.02 g,  $0.10 \times 10^{-3}$  mol) in  $\text{CHCl}_3$  (25 mL) and pyridine (5 mL). After recovery of the low polarity starting material 2 (up to 10%), osmate ester 6 was isolated as a green solid in ~55% yield (~77 mg). 9:  $R_f = 0.25$  (silica,  $\text{CHCl}_3$ );  $^1\text{H}$  NMR (400 MHz,  $\text{CDCl}_3$ ,  $\delta$ ) 8.61 (d,  $^3J = 4.7$  Hz, 1H), 8.59 to 8.48 (m, 5H), 8.44 (d,  $^3J = 4.9$  Hz, 1H), 8.27 (d,  $^3J = 3.4$  Hz, 1H), 7.93 to 7.83 (m, 2H), 7.47–7.33 (m, 4H), 6.82 (s, 2H), –1.28 (br s, 1H), –1.63 (br s, 1H) ppm;  $^{13}\text{C}\{^1\text{H}\}$  NMR (75 MHz,  $\text{CDCl}_3$ ,  $\delta$ ) 168.5, 166.1, 163.7, 152.5, 149.5, 149.4, 141.2, 140.8, 139.2, 138.2, 134.3, 127.6, 127.3, 127.16, 125.18, 122.6, 104.9, 103.0, 101.0, 95.8, 94.4, 88.3 ppm; UV-vis ( $\text{CH}_2\text{Cl}_2$ )  $\lambda_{\text{max}}$  nm (rel intensity) 402 (1.00), 494 (0.07), 529 (0.04), 623 (0.03), 681 (0.25); IR (KBr)  $\nu_{\text{C=O}}$  1766  $\text{cm}^{-1}$ . No molecular peak could be detected in the ESI+ or ESI- MS (100%  $\text{CH}_3\text{CN}$ , 5–30 V cone voltage). The corresponding diol *meso*-tetrakis(pentafluorophenyl)-2,3-cis-dihydroxy-12-oxa-13-oxochlorin was reported previously.<sup>27c</sup>

**Mixture of [meso-Tetrakis(pentafluorophenyl)-2,3-dihydroxy-7-oxa-8-oxochlorinato]platinum(II) Osmate Ester and [meso-Tetrakis(pentafluorophenyl)-2,3-cis-dihydroxy-8-oxa-7-oxochlorinato]platinum(II) Osmate Ester (1:2 mixture of isomers) (14Pt).** Compound 14Pt was prepared according to the general procedure A from 2Pt (100 mg,  $0.08 \times 10^{-3}$  mol), 1 equiv of  $\text{OsO}_4$  (0.02 g,  $0.08 \times 10^{-3}$  mol) in  $\text{CHCl}_3$  (25 mL), and pyridine (5 mL). Product was isolated as a burgundy solid in ~60% yield (~77 mg). 14Pt:  $R_f = 0.25$  (silica,  $\text{CHCl}_3$ );  $^1\text{H}$  NMR (400 MHz,  $\text{CDCl}_3$ ,  $\delta$ ) 8.59 (overlapping d,  $^3J = 5.5$  Hz, 6H – major isomer), 8.49 (d,  $^3J = 5.8$  Hz, 1H – minor isomer), 8.29 (d,  $^3J = 4.9$  Hz, 1H – major isomer), 8.25–8.17 (m, 2H – major isomer), 8.01 (d,  $^3J = 5.1$  Hz, 1H – major isomer), 7.96 to 7.81 (m, 3H – major + minor isomer), 7.50 to 7.34 (m, 4H – major + minor isomer), 6.86 to 6.82 (m, 1H – minor isomer), 6.76 (d,  $^3J = 6.9$  Hz, 1H – major isomer), 6.56 (d,  $^3J = 7.2$  Hz, – major isomer) ppm;  $^{19}\text{F}$  NMR (376 MHz;  $\text{CDCl}_3$ ,  $\delta$ ) –133.8 (dd,  $^3J = 24.01$ , 7.56 Hz, 1F), –134.2 (dd,  $^3J = 23.59$ , 6.83 Hz, 1F), –134.7 (dd,  $^3J = 23.65$ , 6.63 Hz, 1F), –136.9 (overlapping dd, 3F), –137.2 (overlapping dd,  $^3J = 24.98$ , 7.82 Hz, 2F), –138.4 (dd,  $^3J = 23.35$ , 6.99 Hz, 1F), –138.7 (dd,  $^3J = 22.87$ , 7.21 Hz, 1F), –139.0 (overlapping dd,  $^3J = 24.58$ , 7.35 Hz, 2F), –139.7 (dd,  $^3J = 23.75$ , 6.46 Hz, 1F), –151.2 (t,  $^3J = 20.90$  Hz, 1F), –151.85 (t,  $^3J = 16.12$  Hz, 1F), –151.99 (t,  $^3J = 20.81$  Hz, 1F), –153.07 (t,  $^3J = 20.77$  Hz, 1F), –153.24 (t,  $^3J = 21.08$  Hz, 1F), –153.9 (t,  $^3J = 20.89$  Hz, 1F), –160.8 (td,  $^3J = 22.09$ , 7.80 Hz, 1F), –161.0 (td,  $^3J = 21.94$ , 11.06 Hz, 1F), –161.7 (m, 7F), –162.3 (td,  $^3J = 22.57$ , 7.58 Hz, 1F), –163.3 (td,  $^3J = 39.02$ , 17.99 Hz, 2F), –164.0 (td,  $^3J = 22.49$ , 7.27 Hz, 1F) ppm;  $^{13}\text{C}\{^1\text{H}\}$  NMR (101 MHz,  $\text{CDCl}_3$ ,  $\delta$ ) 164.2, 162.9, 152.7, 149.8, 149.6, 146.2, 141.2, 141.0, 138.7, 135.6, 135.2, 131.1, 127.2, 125.5, 125.4, 125.2, 125.0, 113.6, 100.6, 94.5, 93.8, 92.7, 92.1, 85.1 ppm; UV-vis ( $\text{CH}_2\text{Cl}_2$ )  $\lambda_{\text{max}}$  (rel intensity) 390 (1.00), 474 (0.08), 505 (0.06), 548 (0.12), 592 (0.43), 646 (0.04) nm; like all hydroporphyrin osmate esters, no molecular peak could be detected in the ESI+ or ESI- MS (100%  $\text{CH}_3\text{CN}$ , 5–30 V cone voltage).

**1:1 Isomer Mixture of [meso-Tetrakis(pentafluorophenyl)-2,12-dioxa-3,13-dioxoporphyrin] (3<sup>2,13</sup>) and [meso-Tetrakis(pentafluorophenyl)-2,13-dioxa-3,12-dioxoporphyrin] (3<sup>2,12</sup>) Isomers.** The compounds were prepared according to the general procedure C from 7 (30.0 mg,  $0.02 \times 10^{-3}$  mol) and ~10 equiv of CTAP (100 mg,  $0.20 \times 10^{-3}$  mol) with  $\text{CH}_2\text{Cl}_2$  (15 mL) according to the general procedure as a purple solid in ~60% yield (~12 mg). Its spectroscopic properties were identical to those described previously.<sup>4</sup>

**Mixture of [meso-Tetrakis(pentafluorophenyl)-2,7-dioxa-3,8-dioxoporphyrinato]zinc(II), [meso-Tetrakis(pentafluorophenyl)-3,7-dioxa-2,8-dioxoporphyrinato]zinc(II), and [meso-Tetrakis(pentafluorophenyl)-2,8-dioxa-3,7-dioxoporphyrinato]zinc(II).** Path A: The compounds were prepared according to the general procedure C from 12Zn-E/14Zn ( $0.13 \times 10^{-3}$  mol, 240/190 mg) and ~10 equiv of CTAP (1.30  $\times 10^{-3}$  mol) in  $\text{CH}_2\text{Cl}_2$  (10 mL). A mixture of isomers of 4Zn (ratio of 0:1:2 for  $4^{2,8}\text{Zn}$ : $4^{2,7}\text{Zn}$ : $4^{3,7}\text{Zn}$ ) were isolated as a green color solid in ~55–60% yields (~75–80 mg). Path B: The compounds were

prepared according to the general procedure C from 13Zn (30 mg,  $0.03 \times 10^{-3}$  mol) and ~10 equiv of  $\text{CrO}_3$  (30 mg,  $0.30 \times 10^{-3}$  mol) in pyridine (5 mL). The product was isolated as a mixture of isomers (1:2:2 ratios of  $4^{2,8}\text{Zn}$ : $4^{2,7}\text{Zn}$ : $4^{3,7}\text{Zn}$ ) in 30% yield (9 mg) as a greenish blue solid. 4Zn:  $R_f = 0.45$  (silica, 25% hexanes/ $\text{CH}_2\text{Cl}_2$ );  $^1\text{H}$  NMR (400 MHz;  $\text{CDCl}_3$ ,  $\delta$ ) 8.68 (d,  $^3J = 4.8$  Hz, 4H –  $4^{3,7}\text{Zn}$ ), 8.54 (d,  $^3J = 4.8$  Hz, 1H –  $4^{2,7}\text{Zn}$ ), 8.41 (s, 2H –  $4^{2,7}\text{Zn}$ ), 8.39 (d,  $^3J = 4.5$  Hz, 1H –  $4^{2,7}\text{Zn}$ ), 8.32 (d,  $^3J = 4.5$  Hz, 2H –  $4^{2,8}\text{Zn}$ ), 8.19 (d,  $^3J = 4.4$  Hz, 2H –  $4^{2,8}\text{Zn}$ ) ppm;  $^{19}\text{F}$  NMR (376 MHz;  $\text{CDCl}_3$ ,  $\delta$ ) –137.40 to –138.92 (m, 8F), –150.82–151.50 (m, 8F), –160.75 to –161.47 (m 8F) ppm;  $^{13}\text{C}\{^1\text{H}\}$  NMR (101 MHz,  $\text{CDCl}_3$ ,  $\delta$ ) 163.9, 155.9, 152.1, 146.4, 132.2, 128.0, 127.0, 105.7 ppm; UV-vis ( $\text{CH}_2\text{Cl}_2$ )  $\lambda_{\text{max}}$  (log  $\epsilon$ ) 425.0 (5.08), 572.9 (3.84), 622.9 (4.36), 654.2 (3.84) nm; fluorescence emission ( $\lambda_{\text{excitation}} = \lambda_{\text{Soret}}$ ) ( $\text{CH}_2\text{Cl}_2$ )  $\lambda_{\text{max}}$ : 627, 650 nm; IR (neat)  $\nu_{\text{C=O}}$  1771.37  $\text{cm}^{-1}$ ; HR-MS (ESI+, 100%  $\text{CH}_3\text{CN}$ , TOF) calcd for  $\text{C}_{42}\text{H}_{52}\text{F}_{20}\text{N}_4\text{O}_4\text{Zn}$  [M – H]<sup>+</sup> 1072.9277, found 1072.9266.

**Mixture of [meso-Tetrakis(pentafluorophenyl)-2,7-dioxa-3,8-dioxoporphyrinato]platinum(II), [meso-Tetrakis(pentafluorophenyl)-3,7-dioxa-2,8-dioxoporphyrinato]platinum(II), and [meso-Tetrakis(pentafluorophenyl)-2,8-dioxa-3,7-dioxoporphyrinato]platinum(II).** Path A: The compounds were prepared according to the general procedure C from 12Pt-E/14Pt ( $0.13 \times 10^{-3}$  mol, 260/200 mg) and ~10 equiv of CTAP (1.30  $\times 10^{-3}$  mol) in  $\text{CH}_2\text{Cl}_2$  (10 mL). The isomer mixture of 4Pt (ratio of 0:1:2 for  $4^{2,8}\text{Pt}$ : $4^{2,7}\text{Pt}$ : $4^{3,7}\text{Pt}$ ) was isolated as a violet color solid in ~55–60% yield. Path B: The compounds were prepared according to the procedure D from 13Pt (25 mg,  $0.02 \times 10^{-3}$  mol) and ~10 equiv of  $\text{CrO}_3$  (20 mg,  $0.20 \times 10^{-3}$  mol). An isomer mixture of 4Pt (ratio of 1:4:8 for  $4^{2,8}\text{Pt}$ : $4^{2,7}\text{Pt}$ : $4^{3,7}\text{Pt}$ ) was isolated in ~45% yield (11 mg). 4Pt:  $R_f = 0.8$  (silica, 25% hexanes/ $\text{CH}_2\text{Cl}_2$ );  $^1\text{H}$  NMR (400 MHz,  $\text{CDCl}_3$ ,  $\delta$ ) 8.85 (s, 2H –  $4^{2,8}\text{Pt}$ ), 8.70 (s, 2H –  $4^{2,8}\text{Pt}$ ), 8.60 to 8.52 (m, 4H –  $4^{2,7}\text{Pt}$  and 2H –  $4^{2,8}\text{Pt}$ ), 8.44 (d,  $^3J = 5.2$  Hz, 2H –  $4^{2,8}\text{Pt}$ ) ppm;  $^{19}\text{F}$  NMR (376 MHz;  $\text{CDCl}_3$ ,  $\delta$ ) –136.72 to –136.90 (m, 6F), –138.06 to –138.36 (m, 6F), –149.4 (m, 3F), –149.8 (t,  $^3J = 20.17$  Hz, 1F), –150.0 (m, 2F), –159.77 to –160.33 (m, 6F), –160.52 to –160.87 (m, 6F) ppm;  $^{13}\text{C}\{^1\text{H}\}$  NMR (101 MHz,  $\text{CDCl}_3$ ,  $\delta$ ) 161.7, 156.2, 142.5, 137.2, 130.7, 128.0, 117.1, 108.2 ppm; UV-vis ( $\text{CH}_2\text{Cl}_2$ )  $\lambda_{\text{max}}$  (log  $\epsilon$ ) 4.89, 3.95, 4.38, 4.32, 3.95 nm; IR (neat)  $\nu_{\text{C=O}}$  1779.42  $\text{cm}^{-1}$ ; HR-MS (ESI+, 100%  $\text{CH}_3\text{CN}$ , TOF) calcd for  $\text{C}_{42}\text{H}_{52}\text{F}_{20}\text{N}_4\text{O}_4\text{Pt}$  [M + H]<sup>+</sup> 1203.9634, found 1203.9621.

**Direct Oxidation of meso-Tetrakis(pentafluorophenyl)-porphyrin (1): [meso-Tetrakis(pentafluorophenyl)-3,8-dioxa-2,7-dioxoporphyrin] (4<sup>2,7</sup>), [meso-Tetrakis(pentafluorophenyl)-3,7-dioxa-2,8-dioxoporphyrinato] (4<sup>2,8</sup>), [meso-Tetrakis(pentafluorophenyl)-2,8-dioxa-3,7-dioxoporphyrinato] (4<sup>3,7</sup>), and meso-Tetrakis(pentafluorophenyl)-2,3-cis-dihydroxyisobacteriolactone (15).** The compounds were prepared according to the general procedure C from 1 (200 mg,  $0.20 \times 10^{-3}$  mol) and ~10 equiv of CTAP (1.0 g,  $0.20 \times 10^{-3}$  mol). The mixture of isomers of 4 (ratio of 8:8:1 for  $4^{2,8}$ : $4^{2,7}$ : $4^{3,7}$ ) was isolated as the major product in 25% yield (0.20 mmol, 45 mg). *meso*-Tetrakis(pentafluorophenyl)porpholactone 2 was also isolated in 15% yield (30 mg) as a pinkish red solid.<sup>23</sup> In addition, low-polarity starting materials 1 and high-polarity green dihydroxychlorin (5)<sup>27b</sup> and pink dihydroxyisobacteriolactone (15) were isolated each in <5% yield (<10 mg). The regioisomeric isobacteriolactones  $4^{2,8}$ ,  $4^{2,7}$ , and  $4^{3,7}$  were separated from each other in 95% isomer purity after a single pass of preparative TLC (silica–50% hexanes/ $\text{CH}_2\text{Cl}_2$ ).  $4^{2,8}$ :  $R_f = 0.75$  (silica, 25% hexanes/ $\text{CH}_2\text{Cl}_2$ );  $^1\text{H}$  NMR (400 MHz;  $\text{CDCl}_3$ ,  $\delta$ ) 8.71 (d,  $^3J = 2.9$  Hz, 2H), 8.61 (d,  $^3J = 5.1$  Hz, 2H), –0.15 (s, 2H) ppm;  $^{19}\text{F}$  NMR (376 MHz;  $\text{CDCl}_3$ ,  $\delta$ ) –136.9 (d,  $^3J = 15.41$  Hz, 2F), –137.6 (dd,  $^3J = 22.74$ , 7.04 Hz, 2F), –138.3 (dd,  $^3J = 23.05$ , 7.39 Hz, 4F), –148.6 (t,  $^3J = 20.81$  Hz, 1F), –150.3 (t,  $^3J = 21.00$  Hz, 2F), –151.1 (t,  $^3J = 20.90$  Hz, 1F), –159.5 (td,  $^3J = 21.12$ , 10.53 Hz, 2F), –160.8 (td,  $^3J = 21.40$ , 6.17 Hz, 4F), –161.4 (td,  $^3J = 21.57$ , 5.95 Hz, 2F) ppm;  $^{13}\text{C}\{^1\text{H}\}$  NMR (101 MHz;  $\text{CDCl}_3$ ,  $\delta$ ) 164.5, 156.8, 147.2, 144.8, 144.0, 143.0, 141.4, 139.4, 136.8, 136.5, 134.4, 133.2, 132.1, 130.5, 128.0, 125.7, 124.7, 109.4, 105.2, 101.2, 29.7 ppm; UV-vis ( $\text{CH}_2\text{Cl}_2$ )  $\lambda_{\text{max}}$  (log  $\epsilon$ ) 406.5 (5.53), 425.0 (5.53), 526.8 (4.30), 566.2

(4.30), 594.0 (4.40), 640.3 (4.70) nm; fluorescence emission ( $\lambda_{\text{excitation}} = \lambda_{\text{Soret}}$ ) ( $\text{CH}_2\text{Cl}_2$ )  $\lambda_{\text{max}}$ : 645 nm; IR (neat)  $\nu_{\text{C=O}}$  1776.35  $\text{cm}^{-1}$ ;  $\Phi = 0.27$ ; HR-MS (ESI $^+$ , 100%  $\text{CH}_3\text{CN}$ , FTMS) calcd for  $\text{C}_{42}\text{H}_{72}\text{F}_{20}\text{N}_4\text{O}_4$  [M + H] $^+$  1011.0142, found 1011.0151. **4<sup>2,7</sup>**:  $R_f = 0.75$  (silica, 25% hexanes/ $\text{CH}_2\text{Cl}_2$ );  $^1\text{H}$  NMR (400 MHz;  $\text{CDCl}_3$ ,  $\delta$ ) 8.79 (dd,  $J = 5.0$ , 1.9 Hz, 1H), 8.68 (d,  $J = 5.1$  Hz, 1H), 8.65 (d,  $J = 1.6$  Hz, 2H), -0.32 (s, 1H), -0.75 (s, 1H) ppm;  $^{19}\text{F}$  NMR (376 MHz;  $\text{CDCl}_3$ ,  $\delta$ ) -136.82 (dd,  $^3J = 21.24$ , 6.09 Hz, 2F), -136.97 (dd,  $^3J = 22.85$ , 6.84 Hz, 4F), -140.3 (dd,  $^3J = 23.41$ , 7.40 Hz, 2F), -148.7 (t,  $^3J = 20.65$  Hz, 1F), -149.5 (t,  $^3J = 21.00$  Hz, 2F), -152.3 (t,  $^3J = 20.92$  Hz, 1F), -159.6 (td, 2F), -160.2 (td, 4F), -162.2 (td, 2F) ppm;  $^{13}\text{C}\{\text{H}\}$  NMR (101 MHz;  $\text{CDCl}_3$ ,  $\delta$ ) 164.1, 155.8, 152.1, 147.3, 146.4, 144.6, 143.7, 132.1, 128.0, 127.0, 124.4, 29.7, 22.7, 14.1 ppm; UV-vis ( $\text{CH}_2\text{Cl}_2$ )  $\lambda_{\text{max}}$  ( $\log \epsilon$ ) UV-vis ( $\text{CH}_2\text{Cl}_2$ )  $\lambda_{\text{max}}$  ( $\log \epsilon$ ) 408.3 (5.53), 431.2 (5.52), 533.3 (4.30), 585.4 (4.48), 631.2 (4.48); fluorescence emission ( $\lambda_{\text{excitation}} = \lambda_{\text{Soret}}$ ) ( $\text{CH}_2\text{Cl}_2$ ) 635 nm;  $\Phi = 0.34$ ; IR (neat)  $\nu_{\text{C=O}}$  1783.25  $\text{cm}^{-1}$ ; HR-MS (ESI $^+$ , 100%  $\text{CH}_3\text{CN}$ , FTMS) calcd for  $\text{C}_{42}\text{H}_{72}\text{F}_{20}\text{N}_4\text{O}_4$  [M + H] $^+$  1011.0142, found 1011.0151. **4<sup>2,7</sup>**:  $R_f = 0.60$  (silica, 25% hexanes/ $\text{CH}_2\text{Cl}_2$ );  $^1\text{H}$  NMR (400 MHz;  $\text{CDCl}_3$ ,  $\delta$ ) 8.87 (d,  $^3J = 4.7$  Hz, 2H), 8.83 (d,  $^3J = 5.0$  Hz, 2H), -1.99 (s, 2H) ppm;  $^{19}\text{F}$  NMR (376 MHz;  $\text{CDCl}_3$ ,  $\delta$ ) -136.82 (dd,  $^3J = 21.24$ , 6.09 Hz, 2F), -136.97 (dd,  $^3J = 22.85$ , 6.84 Hz, 4F), -140.3 (dd,  $^3J = 23.41$ , 7.40 Hz, 2F), -148.7 (t,  $^3J = 20.65$  Hz, 1F), -149.5 (t,  $^3J = 21.00$  Hz, 2F), -152.3 (t,  $^3J = 20.92$  Hz, 1F), -159.6 (m, 2F), -160.2 (m, 4F), -162.2 (td, 2F) ppm;  $^{13}\text{C}\{\text{H}\}$  NMR (101 MHz;  $\text{CDCl}_3$ ,  $\delta$ ) 164.1, 155.8, 152.1, 147.3, 146.4, 144.6, 143.7, 132.1, 128.0, 127.0, 124.4, 29.7, 22.7, 14.1 ppm; UV-vis ( $\text{CH}_2\text{Cl}_2$ )  $\lambda_{\text{max}}$  ( $\log \epsilon$ ) 418.0 (4.98), 461.8 (3.70), 523.4 (3.48), 572.0 (3.78), 623.8 (4.54) nm; fluorescence emission ( $\lambda_{\text{excitation}} = \lambda_{\text{Soret}}$ ) ( $\text{CH}_2\text{Cl}_2$ ) 625 nm;  $\Phi = 0.12$ ; IR (neat)  $\nu_{\text{C=O}}$  1773.61  $\text{cm}^{-1}$ ; HR-MS (ESI $^+$ , 100%  $\text{CH}_3\text{CN}$ , FTMS) calcd for  $\text{C}_{42}\text{H}_{72}\text{F}_{20}\text{N}_4\text{O}_4$  [M + H] $^+$  1011.0142, found 1011.0152. **15**:  $R_f = 0.42$  ( $\text{CH}_2\text{Cl}_2$ );  $^1\text{H}$  NMR (400 MHz;  $\text{CDCl}_3$ ,  $\delta$ ) 7.92 (d,  $J = 4.8$  Hz, 1H), 7.75 (s, 2H), 7.52 (d,  $J = 4.5$  Hz, 1H), 5.75 (d,  $J = 6.69$ , 1H), 5.64 (d,  $J = 6.83$ , 1H), 3.85 (s, 1H), 2.94 (s, 1H) ppm;  $^{19}\text{F}$  NMR (376 MHz;  $\text{CDCl}_3$ ,  $\delta$ ) -135.6 (d,  $J = 23.54$  Hz, 2F), -137.52 (dd,  $J = 23.48$ , 6.75 Hz, 1F), -137.65 (dd,  $J = 20.65$ , 6.75 Hz, 1F), -138.98 (d,  $J = 16.18$  Hz, 2F), -139.16 (dd,  $J = 23.63$ , 7.44 Hz, 1F), -140.1 (dd,  $J = 3.44$ , 6.67 Hz, 1F), -150.7 (t,  $J = 20.82$  Hz, 1F), -151.5 (t,  $J = 20.80$  Hz, 1F), -151.8 (t,  $J = 21.01$  Hz, 1F), -152.1 (t,  $J = 20.86$  Hz, 1F), -160.5 (td,  $J = 22.12$ , 7.85 Hz, 2F), -161.0 (td,  $J = 22.16$ , 7.68 Hz, 2F), -161.32 (m, 2F), -161.51 (td,  $J = 22.24$ , 11.16 Hz, 1F), -161.69 (td,  $J = 22.34$ , 11.04 Hz, 1F) ppm;  $^{13}\text{C}\{\text{H}\}$  NMR (101 MHz;  $\text{CDCl}_3$ ,  $\delta$ ) 164.6, 162.6, 159.7, 157.6, 155.6, 151.4, 143.55, 143.46, 141.0, 139.1, 136.59, 136.55, 134.9, 134.4, 129.1, 128.2, 127.9, 124.2, 122.4, 112.5, 111.83, 111.65, 110.1, 108.8, 97.7, 86.5, 86.1, 72.4, 71.2, 61.1, 58.0, 29.69, 29.66, 29.59, 19.1, 13.7 ppm; UV-vis ( $\text{CH}_2\text{Cl}_2$ )  $\lambda_{\text{max}}$  ( $\log \epsilon$ ) 385.2 (4.86), 494.4 (3.48), 533.3 (3.90), 575.9 (4.04), 629.6 (3.30) nm; fluorescence emission ( $\lambda_{\text{excitation}} = \lambda_{\text{Soret}}$ ) ( $\text{CH}_2\text{Cl}_2$ )  $\lambda = 587$ , 635 nm;  $\Phi = 0.90$ ; HR-MS (ESI $^+$ , 100%  $\text{CH}_3\text{CN}$ , TOF) calcd for  $\text{C}_{43}\text{H}_{11}\text{F}_{20}\text{N}_4\text{O}_4$  [M + H] $^+$  1027.0455, found 1027.0415.

## ASSOCIATED CONTENT

### Supporting Information

The Supporting Information is available free of charge on the ACS Publications website at DOI: [10.1021/acs.joc.8b02628](https://doi.org/10.1021/acs.joc.8b02628).

UV-vis,  $^1\text{H}$ ,  $^{13}\text{C}$ , and  $^{19}\text{F}$  NMR spectra of all novel compounds; experimental details for the crystal structure determinations of **4<sup>2,7</sup>**, **4<sup>2,8</sup>**, **6**, **7-Z**, **9**, and **12Zn-E**; details for the computations ([PDF](#))

X-ray data for compound **4<sup>2,7</sup>** ([CIF](#))

X-ray data for compound **4<sup>2,8</sup>** ([CIF](#))

X-ray data for compound **6** ([CIF](#))

X-ray data for compound **7-Z** ([CIF](#))

X-ray data for compound **9** ([CIF](#))

X-ray data for compound **12Zn-E** ([CIF](#))

## AUTHOR INFORMATION

### Corresponding Author

\*Tel: +01 (860) 486-2743. E-mail: [c.brückner@uconn.edu](mailto:c.brückner@uconn.edu).

### ORCID

José A. Gascón: [0000-0002-4176-9030](https://orcid.org/0000-0002-4176-9030)

Matthias Zeller: [0000-0002-3305-852X](https://orcid.org/0000-0002-3305-852X)

Christian Brückner: [0000-0002-1560-7345](https://orcid.org/0000-0002-1560-7345)

### Author Contributions

<sup>II</sup>N.H., P.D., and K.S.F.L. contributed equally to this work.

### Notes

The authors declare no competing financial interest.

The X-ray data accession codes for **4<sup>2,7</sup>** (CCDC no. 1867941), **4<sup>2,8</sup>** (CCDC no. 1867939), **6** (CCDC no. 1867938), **7-Z** (CCDC no. 1867943), **9** (CCDC no. 1867940), and **12Zn-E** (CCDC no. 1867942) can also be obtained free of charge from The Cambridge Crystallographic Data Centre via [www.ccdc.cam.ac.uk/data\\_request/cif](http://www.ccdc.cam.ac.uk/data_request/cif)

Oxazolochlorins. 18. Oxazolochlorins 17: see ref 26.

## ACKNOWLEDGMENTS

This work was supported by the US National Science Foundation under Grant Nos. CHE-1465133, CHE-1800361, and CMMI-0730826 (to C.B.), CHE-0754580 (to J.G.), and a graduate fellowship DGE-1247393 (to M.P.G.). The APEX II CCD X-ray diffractometer was funded by NSF Grant CHE-0087210, Ohio Board of Regents Grant CAP-491, and by Youngstown State University. The Quest CMOS X-ray diffractometer was funded by NSF Grant No. CHE-1625543. We thank Randy Hamchand for technical assistance with the HPLC analyses.

## REFERENCES

- Brückner, C. The Breaking and Mending of *meso*-Tetraarylporphyrins: Transmuting the Pyrrolic Building Blocks. *Acc. Chem. Res.* **2016**, *49*, 1080–1092.
- (a) Arnold, L.; Müllen, K. Modifying the Porphyrin Core—a Chemist's Jigsaw. *J. Porphyrins Phthalocyanines* **2011**, *15*, 757–779.  
(b) Lash, T. D. Carbaporphyrins, Porphyrin Isomers and the Legacy of Emanuel Vogel. *J. Porphyrins Phthalocyanines* **2012**, *16*, 423–433.  
(c) Brückner, C.; Akhigbe, J.; Samankumara, L. In *Handbook of Porphyrin Science*; Kadish, K. M., Smith, K. M., Guilard, R., Eds.; World Scientific: River Edge, NY, 2014; Vol. 31, pp 1–276.  
(d) Szyszko, B.; Latos-Grazyński, L. Core Chemistry and Skeletal Rearrangements of Porphyrinoids and Metalloporphyrinoids. *Chem. Soc. Rev.* **2015**, *44*, 3588–3616.  
(e) Costa, L. D.; Costa, J. I.; Tomé, A. C. Porphyrin Macrocycle Modification: Pyrrole Ring-Contracted or -Expanded Porphyrinoids. *Molecules* **2016**, *21*, 320.
- (3) Jayaraj, K.; Gold, A.; Austin, R. N.; Ball, L. M.; Terner, J.; Mandon, D.; Weiss, R.; Fischer, J.; DeCian, A.; Bill, E.; Müther, M.; Schünemann, V.; Trautwein, A. X. Compound I and Compound II Analogues from Porpholactones. *Inorg. Chem.* **1997**, *36*, 4555–4566.
- (4) Ke, X.-S.; Chang, Y.; Chen, J.-Z.; Tian, J.; Mack, J.; Cheng, X.; Shen, Z.; Zhang, J.-L. Porphodilactones as Synthetic Chlorophylls: Relative Orientation of  $\beta$ -Substituents on a Pyrrolic Ring Tunes NIR Absorption. *J. Am. Chem. Soc.* **2014**, *136*, 9598–9607.
- (5) Liang, L.; Lv, H.; Yu, Y.; Wang, P.; Zhang, J.-L. Iron(III) Tetrakis(pentafluorophenyl)porpholactone Catalyzes Nitrogen Atom Transfer to C = C and C-H Bonds with Organic Azides. *Dalton Trans.* **2012**, *41*, 1457–1460.
- (6) Rahimi, R.; Tehrani, A. A.; Fard, M. A.; Sadegh, B. M. M.; Khavasi, H. R. First Catalytic Application of Metal Complexes of Porpholactone and Dihydroxychlorin in the Sulfoxidation Reaction. *Catal. Commun.* **2009**, *11*, 232–235.

(7) Cetin, A.; Ziegler, C. J. Structure and Catalytic Activity of a Manganese(III) Tetraphenylporpholactone. *Dalton Trans.* **2005**, 25–26.

(8) To, W.-P.; Liu, Y.; Lau, T.-C.; Che, C.-M. A Robust Palladium(II)–Porphyrin Complex as Catalyst for Visible Light Induced Oxidative C–H Functionalization. *Chem. - Eur. J.* **2013**, 19, 5654–5664.

(9) (a) Khalil, G. E.; Costin, C.; Crafton, J.; Jones, G.; Grenoble, S.; Gouterman, M.; Callis, J. B.; Dalton, L. R. Dual-Luminophor Pressure-Sensitive Paint I. Ratio of Reference to Sensor Giving a Small Temperature Dependency. *Sens. Actuators, B* **2004**, 97, 13–21. (b) Zelelow, B.; Khalil, G. E.; Phelan, G.; Carlson, B.; Gouterman, M.; Callis, J. B.; Dalton, L. R. Dual Luminophor Pressure Sensitive Paint II. Lifetime Based Measurement of Pressure and Temperature. *Sens. Actuators, B* **2003**, 96, 304–314. (c) Gouterman, M.; Callis, J.; Dalton, L.; Khalil, G.; Mebarki, Y.; Cooper, K. R.; Grenier, M. Dual Luminophor Pressure-Sensitive Paint: III. Application to Automotive Model Testing. *Meas. Sci. Technol.* **2004**, 15, 1986–1994.

(10) Ke, X. S.; Yang, B. Y.; Cheng, X.; Chan, S. L. F.; Zhang, J. L. Ytterbium(III) Porpholactones:  $\beta$ -Lactonization of Porphyrin Ligands Enhances Sensitization Efficiency of Lanthanide Near-Infrared Luminescence. *Chem. - Eur. J.* **2014**, 20, 4324–4333.

(11) Worlinsky, J. L.; Halepas, S.; Brückner, C. PEGylated *meso*-Arylporpholactone Metal Complexes as Optical Cyanide Sensors in Water. *Org. Biomol. Chem.* **2014**, 12, 3991–4001.

(12) Wu, Z.-Y.; Wang, T.; Meng, Y.-S.; Rao, Y.; Wang, B.-W.; Zheng, J.; Gao, S.; Zhang, J.-L. Enhancing the Reactivity of Nickel(II) in Hydrogen Evolution Reactions (HERs) by  $\beta$ -Hydrogenation of Porphyrinoid Ligands. *Chem. Sci.* **2017**, 8, 5953–5961.

(13) Liu, E.; Ghandehari, M.; Brückner, C.; Khalil, G.; Worlinsky, J.; Jin, W.; Sideley, A.; Hyland, M. A. Mapping High pH Levels in Hydrated Calcium Silicates. *Cem. Concr. Res.* **2017**, 95, 232–239.

(14) Tang, J.; Chen, J.-J.; Jing, J.; Chen, J.-Z.; Lv, H.; Yu, Y.; Xu, P.; Zhang, J.-L.  $\beta$ -Lactonization of Fluorinated Porphyrin Enhances LDL Binding Affinity, Cellular Uptake with Selective Intracellular Localization. *Chem. Sci.* **2014**, 5, 558–566.

(15) Yoshida, K.; Osuka, A. Subporpholactone Subporpholactam, Imidazolosubporphyrin, and Iridium Complexes of Imidazolosubporphyrin: Formation of Iridium Carbene Complexes. *Angew. Chem., Int. Ed.* **2018**, 57, 338–342.

(16) Gouterman, M.; Hall, R. J.; Khalil, G. E.; Martin, P. C.; Shankland, E. G.; Cerny, R. L. Tetrakis(Pentafluorophenyl)-Porpholactone. *J. Am. Chem. Soc.* **1989**, 111, 3702–3707.

(17) Yu, Y.; Lv, H.; Ke, X.; Yang, B.; Zhang, J.-L. Ruthenium-Catalyzed Oxidation of the Porphyrin  $\beta,\beta'$ -Pyrrolic Ring: A General and Efficient Approach to Porpholactones. *Adv. Synth. Catal.* **2012**, 354, 3509–3516.

(18) Crossley, M. J.; King, L. G. Novel Heterocyclic Systems from Selective Oxidation at the  $\beta$ -Pyrrolic Position of Porphyrins. *J. Chem. Soc., Chem. Commun.* **1984**, 920–922.

(19) Wang, X.; Nurtila, S. S.; Dzik, W. I.; Becker, R.; Rodgers, J.; Reek, J. N. H. Tuning the Porphyrin Building Block in Self-Assembled Cages for Branched-Selective Hydroformylation of Propene. *Chem. - Eur. J.* **2017**, 23, 14769–14777.

(20) (a) Kikuchi, G.; Yoshida, T.; Noguchi, M. Heme Oxygenase and Heme Degradation. *Biochem. Biophys. Res. Commun.* **2005**, 338, 558–567. (b) Kräutler, B. Breakdown of Chlorophyll in Higher Plants—Phyllobilins as Abundant, yet Hardly Visible Signs of Ripening, Senescence, and Cell Death. *Angew. Chem., Int. Ed.* **2016**, 55, 4882–4907.

(21) Lv, H.; Yang, B.; Jing, J.; Yu, Y.; Zhang, J.; Zhang, J.-L. Dual Facet of Gold(III) in the Reactions of Gold(III) and Porphyrins. *Dalton Trans.* **2012**, 41, 3116–3118.

(22) The naming/numbering system for the specific isomers used is derived from the formal numbering of the position of their oxo groups. This nomenclature varies from the IUPAC nomenclature for chlorins: Moss, G. P. *Pure Appl. Chem.* **1987**, 59, 779–832.

(23) Brückner, C.; Ogikubo, J.; McCarthy, J. R.; Akhigbe, J.; Hyland, M. A.; Daddario, P.; Worlinsky, J. L.; Zeller, M.; Engle, J. T.; Ziegler, C. J.; Ranaghan, M. J.; Sandberg, M. N.; Birge, R. R. *meso*-Arylporpholactones and Their Reduction Products. *J. Org. Chem.* **2012**, 77, 6480–6494.

(24) Wan, J. R.; Gouterman, M.; Green, E.; Khalil, G. E. High Performance Liquid Chromatography Separation and Analysis of Metalloc Tetra(pentafluorophenyl)porpholactone. *J. Liq. Chromatogr.* **1994**, 17, 2045–2056.

(25) Brückner, C.; Samankumara, L.; Ogikubo, J. In *Handbook of Porphyrin Science*; Kadish, K. M., Smith, K. M., Guilard, R., Eds.; World Scientific: River Edge, NY, 2012; Vol. 17, pp 1–112.

(26) Hewage, N.; Zeller, M.; Brückner, C. Oxidations of Chromene-Annulated Chlorins. *Org. Biomol. Chem.* **2017**, 15, 396–407.

(27) (a) Samankumara, L. P.; Zeller, M.; Krause, J. A.; Brückner, C. Syntheses, Structures, Modification, and Optical Properties of *meso*-Tetraaryl-2,3-Dimethoxychlorin, and Two Isomeric *meso*-Tetraaryl-2,3,12,13-Tetrahydroxybacteriochlorins. *Org. Biomol. Chem.* **2010**, 8, 1951–1965. (b) Hyland, M. A.; Morton, M. D.; Brückner, C. *meso*-Tetra(pentafluorophenyl)porphyrin-Derived Chromene-Annulated Chlorins. *J. Org. Chem.* **2012**, 77, 3038–3048. (c) Hyland, M. A.; Hewage, N.; Panther, K.; Nimthong Roldan, A.; Zeller, M.; Samaraweera, M.; Gascon, J. A.; Brückner, C. Chromene-Annulated Bacteriochlorins. *J. Org. Chem.* **2016**, 81, 3603–3618.

(28) (a) Schröder, M. Osmium Tetroxide *cis*-Hydroxylation of Unsaturated Substrates. *Chem. Rev.* **1980**, 80, 187–213. (b) Hawkins, J. M.; Meyer, A.; Lewis, T. A.; Loren, S.; Hollander, F. J. Crystal Structure of Osmylated C<sub>60</sub>: Confirmation of the Soccer Ball Framework. *Science* **1991**, 252, 312–313.

(29) Shelton, J. A.; Song, X.-Z.; Ma, J.-G.; Jentzen, W.; Medforth, C. J. Nonplanar Porphyrins and their Significance in Proteins. *Chem. Soc. Rev.* **1998**, 27, 31–41.

(30) Lau, K. S. F., Ph.D. Thesis, University of Washington, 2006.

(31) Akhigbe, J.; Haskoor, J. P.; Krause, J. A.; Zeller, M.; Brückner, C. Formation, Structure and Reactivity of *meso*-Tetraaryl-Chlorolactones, -Porpholactams, and Chlorolactams, Porphyrin and Chlorin Analogues Incorporating Oxazolone or Imidazolone Moieties. *Org. Biomol. Chem.* **2013**, 11, 3616–3628.

(32) Yu, Y.; Furuyama, T.; Tang, J.; Wu, Z.-Y.; Chen, J.-Z.; Kobayashi, N.; Zhang, J.-L. Stable Iso-Bacteriochlorin Mimics from Porpholactone: Effect of a  $\beta$ -Oxazolone Moiety on the Frontier  $\pi$ -Molecular Orbitals. *Inorg. Chem. Front.* **2015**, 2, 671–677.

(33) (a) Bruhn, T.; Brückner, C. Origin of the Regioselective Reduction of Chlorins. *J. Org. Chem.* **2015**, 80, 4861–4868. (b) Almeida, J.; Aguiar, A.; Leite, A.; Silva, A. M. N.; Cunha-Silva, L.; de Castro, B.; Rangel, M.; Barone, G.; Tome, A. C.; Silva, A. M. G. 1,3-Dipolar Cycloadditions with *meso*-Tetraarylchlorins – Site Selectivity and Mixed Bisadducts. *Org. Chem. Front.* **2017**, 4, 534–544.

(34) Brückner, C.; Dolphin, D.  $\beta,\beta'$ -Dihydroxylation of *meso*-Tetraphenylchlorins and Metallocchlorins. *Tetrahedron Lett.* **1995**, 36, 9425–9428.

(35) Khalil, G.; Gouterman, M.; Ching, S.; Costin, C.; Coyle, L.; Gouin, S.; Green, E.; Sadilek, M.; Wan, R.; Yearyan, J.; Zelelow, B. Synthesis and Spectroscopic Characterization of Ni, Zn, Pd and Pt Tetra(pentafluorophenyl)porpholactone with Comparison to Mg, Zn, Y, Pd and Pt Metal Complexes of Tetra(pentafluorophenyl)porphine. *J. Porphyrins Phthalocyanines* **2002**, 6, 135–145.

(36) Stolzenberg, A. M.; Spreer, L. O.; Holm, R. H. Octaethylisobacteriochlorin, a Model of the Sirohydrochlorin Ring System of Siroheme Enzymes: Preparation and Spectroscopic and Electrochemical Properties of the Free Base and its Zn(II) Complex. *J. Am. Chem. Soc.* **1980**, 102, 364–370.

(37) Dash, S.; Patel, S.; Mishra, B. K. Oxidation by Permanganate: Synthetic and Mechanistic Aspects. *Tetrahedron* **2009**, 65, 707–739.

(38) Stepien, M.; Latos-Grazynski, L. Aromaticity and Tautomerism in Porphyrins and Porphyrinoids. *Top. Heterocycl. Chem.* **2009**, 19, 83–153.

(39) (a) Becke, A. D. Density-Functional Thermochemistry. III. The Role of Exact Exchange. *J. Chem. Phys.* **1993**, 98, 5648–5652. (b) Stephens, P.; Devlin, F.; Chabalowski, C.; Frisch, M. J. Ab Initio

Calculation of Vibrational Absorption and Circular Dichroism Spectra Using Density Functional Force Fields. *J. Phys. Chem.* **1994**, *98*, 11623–11627.

(40) (a) Barone, V.; Cossi, M. Quantum Calculation of Molecular Energies and Energy Gradients in Solution by a Conductor Solvent Model. *J. Phys. Chem. A* **1998**, *102*, 1995–2001. (b) Cossi, M.; Rega, N.; Scalmani, G.; Barone, V. Energies, Structures, and Electronic Properties of Molecules in Solution with the C-PCM Solvation Model. *J. Comput. Chem.* **2003**, *24*, 669–681.

(41) Frisch, M. J.; Trucks, G. W.; Schlegel, H. B.; Scuseria, G. E.; Robb, M. A.; Cheeseman, J. R.; Scalmani, G.; Barone, V.; Mennucci, B.; Petersson, G. A.; Nakatsuji, H.; Caricato, M.; Li, X.; Hratchian, H. P.; Izmaylov, A. F.; Bloino, J.; Zheng, G.; Sonnenberg, J. L.; Hada, M.; Ehara, M.; Toyota, K.; Fukuda, R.; Hasegawa, J.; Ishida, M.; Nakajima, T.; Honda, Y.; Kitao, O.; Nakai, H.; Vreven, T.; Montgomery, J. A., Jr.; Peralta, J. E.; Ogliaro, F.; Bearpark, M. J.; Heyd, J.; Brothers, E. N.; Kudin, K. N.; Staroverov, V. N.; Kobayashi, R.; Normand, J.; Raghavachari, K.; Rendell, A. P.; Burant, J. C.; Iyengar, S. S.; Tomasi, J.; Cossi, M.; Rega, N.; Millam, N. J.; Klene, M.; Knox, J. E.; Cross, J. B.; Bakken, V.; Adamo, C.; Jaramillo, J.; Gomperts, R.; Stratmann, R. E.; Yazyev, O.; Austin, A. J.; Cammi, R.; Pomelli, C.; Ochterski, J. W.; Martin, R. L.; Morokuma, K.; Zakrzewski, V. G.; Voth, G. A.; Salvador, P.; Dannenberg, J. J.; Dapprich, S.; Daniels, A. D.; Farkas, Ö.; Foresman, J. B.; Ortiz, J. V.; Cioslowski, J.; Fox, D. J. *Gaussian 09*; Gaussian, Inc.: Wallingford, CT, 2009.

(42) Jentzen, W.; Song, X.-Z.; Shelnutt, J. A. Structural Characterization of Synthetic and Protein-Bound Porphyrins in Terms of the Lowest-Frequency Normal Coordinates of the Macrocycle. *J. Phys. Chem. B* **1997**, *101*, 1684–1699.

(43) Spellane, P. J.; Gouterman, M.; Antipas, A.; Kim, S.; Liu, Y. C. Electronic Spectra and Four-Orbital Energies of Free-Base, Zinc, Copper, and Palladium Tetrakis(perfluorophenyl)porphyrins. *Inorg. Chem.* **1980**, *19*, 386–391.

(44) Buchler, J. W. In *The Porphyrins*; Dolphin, D., Ed.; ScienceDirect, 1978; Vol. 1, pp 389–483.

(45) Kumar, P. H.; Venkatesh, Y.; Prashanthi, S.; Siva, D.; Ramakrishna, B.; Bangal, P. R. Diffusive and Non-Diffusive Photo-Induced Proton Coupled Electron Transfer from Hydrogen Bonded Phenols to *meso*-Tetrakis-5,10,15,20-Pentafluorophenyl Porphyrin. *Phys. Chem. Chem. Phys.* **2014**, *16*, 23173–23181.